SCINTILLATION AND BIT ERROR RATE PERFORMANCE COMPARISON OF BOTTLE AND SINE HOLLOW BEAMS

MERT BAYRAKTAR

DECEMBER 2019

SCINTILLATION AND BIT ERROR RATE PERFORMANCE COMPARISON OF BOTTLE AND SINE HOLLOW BEAMS

A THESIS SUBMITTED TO
THE GRADUATE SCHOOL OF NATURAL AND APPLIED
SCIENCES OF
ÇANKAYA UNIVERSITY

BY
MERT BAYRAKTAR

IN PARTIAL FULFILLMENT OF THE REQUIREMENTS FOR THE
DEGREE OF
DOCTORATE OF PHILOSOPHY
IN
THE DEPARTMENT OF
ELECTRONIC AND COMMUNICATION ENGINEERING

DECEMBER 2019

Title of the Thesis: **Scintillation and bit error rate performance comparison of bottle and sine hollow beams**

Submitted by **Mert BAYRAKTAR**

Approval of the Graduate School of Natural and Applied Sciences, Çankaya University.

Prof. Dr. Can ÇOĞUN
Director

I certify that this thesis satisfies all the requirements as a thesis for the degree of Doctorate of Philosophy

Prof. Dr. Sıtkı Kemal İDER
Head of Department

This is to certify that we have read this thesis and that in our opinion it is fully adequate, in scope and quality, as a thesis for the degree of Doctorate of Philosophy

Prof. Dr. Halil Tanyer EYYUBOĞLU
Supervisor

Examination Date: 06.12.2019

Examining Committee Members

Prof. Dr. Fırat HARDALAÇ	Gazi Univ.	
Prof. Dr. Halil Tanyer EYYUBOĞLU	Karatekin Univ.	
Dr. Ins. Özgür ERGÜL	Atılım Univ.	
Dr. Ins. Serap ALTAY ARPALİ	Çankaya Univ.	
Dr. Ins. Emre SERMUTLU	Çankaya Univ.	

STATEMENT OF NON-PLAGIARISM PAGE

I hereby declare that all information in this document has been obtained and presented in accordance with academic rules and ethical conduct. I also declare that, as required by these rules and conduct, I have fully cited and referenced all material and results that are not original to this work.

Name, Last Name : Mert BAYRAKTAR

Signature :

Date : 06.12.2019

ABSTRACT

Scintillation and Bit Error Rate Performance Comparison of Bottle and Sine Hollow Beams

BAYRAKTAR, Mert

Phd., Department of Electronic and Communication Engineering

Supervisor: Prof. Dr. Halil Tanyer EYYUBOĞLU

December 2019, 79 pages

This thesis involves scintillation behavior, and probability of error estimation of optical wireless communication links using bottle and sine hollow beams on the source plane. In addition to performance over communication link, propagation and kurtosis parameter of bottle beams are analyzed as well. Analytical derivation of scintillation of bottle beam is performed utilizing Rytov scintillation theory. Since equations becomes too complicated to solve intensity profiles, kurtosis parameter, scintillation estimation, and probability of error values of selected bottle beams are obtained benefiting from random phase screen approach. Utilizing the same method, scintillation index and bit error rate(BER) of sine hollow beam are evaluated too. Our results show that asymmetric bottle beams have less scintillation value under the same conditions as compared to corresponding symmetric ones. This brings us, asymmetric bottle beams have less bit error rate when signal to noise ratio is constant. Since, scintillation index of sine hollow beam becomes less than Gaussian beam in weak turbulence, this beam seems advantageous considering BER for weak turbulence. Scintillation results are compared with spherical wave and obtained probability of error values are compared with the analytical formula and plotted in this study.

Keywords: Scintillation, bottle beam, sine hollow beam, bit error rate, turbulence.

ÖZ

Şişe ve Sinus Oyuk Işınlarının Parıldama ve Bit Hata Oranı Performansı Karşılaştırması

BAYRAKTAR, Mert

Doktora, Elektronik ve Haberleşme Mühendisliği Anabilim Dalı

Tez Yöneticisi: Prof. Dr. Halil Tanyer EYYUBOĞLU

Aralık 2019, 79 sayfa

Bu çalışma kaynak düzleminde şişe ve sinus oyuk ışınları kullanan kablosuz optik haberleşme hatlarında parıldama davranışı ve hata olasılığı tahminini içermektedir. Haberleşme linki üzerindeki performasına ek olarak, şişe ışınının yayılma ve kurtosis parametresi de analiz edilmiştir. Şişe ışının parıldamasının analitik türetimi Rytov parıldama teorisinden faydalanarak yapılmıştır. Denklemler çözülmesi çok zor olduğundan yayılma özellikleri, kurtosis parametresi, parıldama tahmini ve hata olasılığı değerleri rastgele faz tabakaları yöntemi kullanılarak elde edilmiştir. Aynı merthodu kullanara sinus oyuk ışınının da parıldama ve bit hata oranı hesaplanmıştır. Sonuçlarımız gösteriyor ki, asimetrik şişe ışınlarının parıldaması aynı şartlarda karşılık gelen simetrik ışınlara nazaran daha azdır. Bu da bize asimetrik ışınların sabit sinyal gürültü oranında daha düşük bit hata oranına sahip olduğunu sonucunu getirmektedir. Zayıf türbülansta sinüs oyuk ışınının parıldaması Gaussian ışınından daha az olduğu için, bu ışın zayıf türbülansta bit hata oranı bakımından daha vantajlı görünmektedir. Parıldama sonuçları küresel dalga ile karşılaştırılmış ve elde edilen hata olasılığı değerleri analitik formül ile kaşılaştırılıp bu çalışmada çizilmiştir.

Anahtar Kelimeler: Parıldama, şişe ışını,sinus oyuk ışını, bit hata oranı, türbülans.

ACKNOWLEDGEMENTS

TABLE OF CONTENTS

LIST OF FIGURES

FIGURES

FIGURES

FIGURES

LIST OF ABBREVIATIONS

FSO   Free Space Optics

RPS   Random Phase Screen

BB   Bottle Beam

SHB   Sine Hollow Beam

GB   Gaussian Beam

BER   Bit Error Rate

Pe   Probability of Error

SNR   Signal to Noise Ratio

OWC   Optical Wireless Communication

CHAPTER 1

INTRODUCTION

In our developing world, nowadays we plan to move on to fifth generation GSM system 5G. In 5G, it is planned that latency all over the world will below 1ms. To reach this value, optical networks gain importance. Free space optic(FSO) is one of the types of optical wireless communication(OWC) system which establishes wireless communication through the atmosphere. Since channel of these communication systems is atmosphere, performance of these systems is strongly dependent on the atmospheric turbulence. In commercial FSO systems, laser diodes are used and intensity distribution of these lasers have Gaussian distribution. Because of this distribution, output beam is called as Gauss beam. Gauss beam have handicap in strong turbulent conditions. One of ways to improve performance of FSO systems lie behind intensity distribution of transmitter laser. Non-conventional beams can improve performance of OWC systems and some of them are listed in below "Literature Review" section. Based on these studies, we prepare this thesis to show how we can improve performance of OWC systems using bottle beam and sine hollow beam.

1.1 Literature Review

Beam shaping is one of the trend topics of our developing science world. Beams having different intensity profiles than Gaussian beam are studied in several studies for different applications. Starting from this point, optical bottle beam is introduced in [1] as superposition of two Laguerre modes. Theoretical background of bottle beam is explained starting from Hankel functions and lens system is designed for three dimensional beam in [2]. In another study [3], scientists show that bottle beam

can be generated passing Bessel beam through an aperture. Another technique to generate bottle beam is usage of axicon. In [4], authors indicate that bottle beam and hollow beams are generated instead of Bessel beam if focal length of axicon is less than axial region. Multi-ring hollow Gaussian beam is set as initial point to generate bottle beam in [5]. In this study, scientists design a lens system and benefit from spherical aberration. Bottle beam is also generated utilizing Bessel correlated schell model vortex beams in [6]. In this paper, authors indicate that vortex bottle beam carries orbital angular momentum in addition to other advantages. Super Gaussian beam is chosen as initial beam for lens system in [7] and it is shown that distance between lens and axicon effects the width of hollow region of beam. Similarly, effect of distance between lens and axicon is studied in [8]. Polarization is added to bottle beam in [9] and scientists present that azimuthal polarized beam is obtained with high numerical aperture lens. In addition, Azimuthal and radial polarized beam can be obtained if numerical aperture of lens is less than 0.1. Usage of fiber cables is another technique to generate bottle beams. Supercontinuum(SC) fibers and axicons are used to generated bottle beams in [10] with the support of Fresnel Kirchoff formula. Generating Bessel beams with different orders using fiber is another method to generate bottle beam [11]. It is possible to generate bottle beams via sound effect. In [12], it is shown that bottle beam can be generated using acousto optic method. Make use of self-image property, hollow width is set in [13]. Using spatial frequency optimization technique, effective length of bottle beam is increased benefiting from self-imaging property [14]. Experimental set-up is established in [15], size and uniformity of beam is determined based upon structure of vortex. Array bottle beams are generated using a diffractive optical element in [16]. Partially coherent form of bottle beams is generated changing the spatial degree of coherence of initial beam in [17]. Setting topological charge, coherence length, and radial frequency, partially coherent vortex bottle beam is generated in [18]. There are also another types of bottle beams such as non-paraxial and plasmonic. It is shown in [19] how to generate microscale non-paraxial bottle beam. In [20], plasmonic bottle beam is obtained mounting cos-Gaussian beam. It is used self-accelerating of surface-plasmon beams to generate plasmonic bottle beams in [21]. Finally, bottle beam is directly generated

using an end pumped Nd:YVO4 laser and they show that these beams can overcome the high refractive index mediums [22].

The other selected beam for this thesis is sine hollow beam. This type of beam is defined in [23] and its intensity profile is examined in detail along the propagation path.

Propagation of different beams through free space or turbulent atmosphere draws the attention of several scientists. For this purpose, they applied some techniques such as ABCD matrix, Huygens-Fresnel integral, and random phase screen(RPS) approach. Applying these techniques, it is possible to have intensity distribution, phase distribution, Kurtosis parameter, beam size variations or scintillation behavior of beams. Authors studied propagation of asymmetric tunable dual airy beams through ABCD system in [24]. They give the analytical expression of propagation too. Using ABCD matrix, scientists [25] show that controllable hollow flat-topped beam turns into Gaussian beam in closer distances under stronger turbulence than free space. Propagation properties of truncated Mathieu beams using Collins formula and ABCD matrix is studied in [26]. In similar study, scientists show that Mathieu Gaussian beams have focalization property [27]. Andrew presents Huygens-Fresnel integral which gives the exact solution of propagated field in [28]. It is shown in [29] that beam propagation factor of radial Gaussian Schell Model beam is independent of beam number however it is directly proportional to radius of rings. Analytically, it is stated in [30] that vortexity of partially coherent Bessel-Gaussian beam is affected less if topological charge increases. Airy beam turns into Gaussian beam and spreading increases when turbulent increases in [31]. Benefiting from Huygens-Fresnel integral, scientists make a comparison between focused vector laser beam and collimated vector laser beams considering irradiance, spreading, and polarization in [32]. Schmidt introduces a numerical method which is called as random phase screen to simulate atmosphere in [33]. Based upon this technique, authors of this paper show that cylindrical-sinc Gaussian beam have generally off axis behavior and its Kurtosis parameter has a decaying profile [34].

One of the important parameters of beams along propagation path is Kurtosis parameter. That's why, some scientists carried out their studies on this topic. Kurtosis parameters are introduced in [35] and possible behaviors are shown. Effect

of convergent and divergent axicons are studied in [36] and it is resulted as Kurtosis parameter has the same absolute value for both cases. Formulation of different types of Kurtosis parameter for general beams is given in [37] and Kurtosis parameters of ince-Gaussian beam show nearly raising behavior. It is investigated in [38] that Kurtosis parameter of Bessel modulated Gaussian beams depends on beam order, Rayleigh length, and A/B parameters in ABCD system. Scientists illustrate that Kurtosis parameter of flat-topped Gaussian beams are dependent on refractive index of medium in [39]. Kurtosis parameters of elegant Hermite-Gaussian beam and Laguerre Gaussian beam is evaluated in [40] and it is shown that it shows stable plot for orders 0,1 of elegant Hermite-Gaussian beam and order 0 for Laguerre Gaussian beam. Without considering, propagation distance, wavelength, and inner scales beam wander of Airy beam is stable against Kurtosis parameter in [41]. Analytical derivation of Kurtosis parameter for Lorentz beam is performed and it is resulted as it has decaying profile up to some distance and then it raises [42]. The authors investigate in [43] that Kurtosis parameter of Hermite-cosh-Gaussian beam are affected by beam order, decentered parameter, and Fresnel number. Finally, it is significantly resulted that Kurtosis parameter of a broadband system raises when bandwidth increases in [44].

Scintillation is the most important noise factor in optical wireless communication in turbulent atmosphere. Tatarski derived the log amplitude variance of spherical wave in [45]. Fried emphasize that scintillation reduces when aperture opening increases [46]. Irradiance fluctuations of Gaussian beam is derived in [47]. Variance of scintillation noise is the most dominant one comparing with shot and thermal noise as it is demonstrated in [48]. Scintillation index of various beams also take place in literature. It is mentioned in [49] that astigmatic annular beam has less scintillation than Gaussian beam. Applying very well-known Rytov method, scintillation expression of airy beam is derived in [50]. It is declared in [51] that partially coherent beams have less scintillation among annular, cosh, and cos Gaussian beam. Scintillation index of hypergeometric Gaussian beam is studied in [52] utilizing random phase screen approach. It is resulted as on axis scintillation index decreases while hollowness parameter increases for small Gaussian source sizes. Another study [53] with random phase screen shows that annular beam is the

4

best among sinusoidal and hyperbolic Gaussian beam. It is mentioned in [54] that annular Gaussian and dark hollow beam has better performance than Gaussian beam in terms of scintillation. Similar with our results, scintillation index of asymmetric annular and flat topped beams is lower than Gaussian beam [55]. It is shown in [56] that asymmetric form of annular beam has lower scintillation than spherical wave.

Orbital angular momentum is the technique to carry information via topological charge. In recent years, orbital angular momentum becomes popular. There are several studies indicates that orbital angular momentum increases the link capacity. 16-QAM is multiplexed with OAM and 1 Tbps link is established in [57]. Another 600m link which has 100 Ghz bandwidth is set generating OAM with SLM in [58]. Different type of beams having vortex are used in OAM applications. 1 bit OAM vortex beam generator is designed in [59]. Authors use Laguerre Gaussian beam starting from Nd:YVO4 laser in [60] and analyze the phase structure of generated beam. Scientists indicates that security and performance of communication system can increase using elliptic vortex beam [60]. It is strongly mentioned in [61] that increase in the topological charge does not vanish the information in communication link if perfect optical vortex beam is used. Benefiting from Rytov theory, they study on detection probability of Airy-OAM beam. They show that beam with small topological charge becomes resistive to oceanic turbulence [62]. It is resulted in [63] that OAM shift keying decoder is efficient if Laguerre Gaussian beam is used in oceanic turbulence which is simulated with random phase screen. Authors indicate that first experimental study is carried out in [64]. Turbulence effect over OAM modes can be reduced using adaptive optics as it is said in [65]. In addition to adaptive optics, a beacon is added to communication system with OAM [66]. In another experimental set-up is established and OAM is used with wavelength division multiplexing in [67]. Related with detection of OAM, authors indicate in [68] that phase information can be detected if common path interferometer is used. Combination of incoherent superposition and multiplexing phase hologram technique show good performance in [69]. In addition to topological charge, data is carried via combination of phase and amplitude in [70]. Authors investigate that probability of error of this system underneath the forward error correction limit.

Probability of error plays key role to measure the performance of communication system. That's why, several scientists focus on this value to improve. Numerical study [71] is carried out based upon scintillation and beam wandering effect. It is found in [72] that flattened Gaussian beam shows better performance than Gaussian beam in terms of bit error rate(BER). Theoretical formula of BER considering noise variance is given in [73]. Effect of scintillation over probability of error is studied in [74] and it is resulted as probability of error is inversely proportional to irradiance fluctuations. BER of FSO system applying binary phase shift keying (PSK) is studied in [75]. There are some methods to decrease the probability of error in FSO systems such as encoding, applying different modulation types, and beam shaping. In the comparison of low density parity check (LDPC) codes and Reed Solomon codes in [76], LDPC codes have less probability of error under gamma gamma distributed atmosphere. Performance analysis of RF hybrid FSO system is done applying LDPC codes [77]. On-off keying (OOK) has the best performance compared to quadrature phase shift keying (QPSK) and 16 PSK in [78]. Another hybrid system is established with wire in [79]. Scientists show that effect of turbulence reduces applying hybrid system. BER comparison among OOK, differential phase shift keying (DPSK), and differential quadrature phase shift keying (DQPSK) is studied in [80] and authors indicate that performance of all modulation techniques gets better if space diversity reception technique is applied. A physical experiment set-up is established to measure the performance of OAM multiplexed system in [81]. Effect of adaptive optics is studied in two parts [82-83]. Lower order adaptive optics systems decrease BER 42 times however higher order reduces 41.5 times. Probability of error of Gaussian Schell model beam is derived in [84]. Variations of number of detectors over BER behavior also attract the attention of scientists. It is shown in [85] that probability of error of FSO system with array detector is less than single detector one. Similarly, small array detectors have better performance as compared to single large detector considering probability of error in [86]. Scientists indicate in [87] that it can be reached   BER value if avalanched photodiode gain is 700 and 60 photons are caught per bit. Finally, author of this thesis indicates probability of error of truncated Bessel beam is inversely proportional to beam order [88].

1.2 Scope and Objectives

In this thesis, effect of Bottle beam on FSO link is studied. To do this, scintillation expression of Bottle beam is derived using Rytov theory. Applying random phase screen approach, intensity profiles of symmetric and asymmetric cases after propagation is obtained. Additionally, Kurtosis parameter which shows sharpness of the beam is evaluated numerically and explain the relationship between scintillation index. Scintillation index of all selected bottle beams are evaluated utilizing RPS and compared with Gaussian beam. Comparisons are made for point-like and aperture averaged scintillation with small and large receiver apertures. Then, effect of scintillation over signal to noise ratio and probability of error is analyzed in detail.

In case of sine hollow beam, scintillation is analyzed considering both point like and aperture averaged conditions. In addition, bit error rate of sine hollow beam is examined depending on atmospheric turbulence condition and received SNR.

1.3 Organization of the Thesis

We divide this thesis into six chapters. Our main purpose is to obtain scintillation and probability of error in the propagation through turbulent atmosphere present bottle beam and sine hollow beam.

Chapter 1 includes literature review, objective of this thesis and organization part.

Chapter 2 shows intensity and phase distributions on the source plane and gives analytical expression for scintillation.

Chapter 3, explains simulation environment.

Chapter 4 indicates the intensity and phase profiles after propagation and kurtosis parameter of bottle beam.

In Chapter 5, we show scintillation and probability of error performance of bottle beam.

Chapter 6 involves scintillation and probability of error performance of sine hollow beam and its comparison with bottle beam.

7

Chapter 7 is the conclusion of this thesis.

CHAPTER 2

SCINTILLATION EXPRESSION OF BOTTLE BEAM VIA RYTOV METHOD

In this part of paper, bottle beam with different settings is introduced. Then scintillation index via Rytov scintillation theory is derived up to las integral part.

2.1 Source Field Distribution of Bottle Beam

Source field expression of bottle beam is taken from [89] as

$$u_s(s) = u_s(s_x, s_y) = \left[\frac{-(s_x^2 + s_y^2)^2}{2a_{sx}^2 a_{sy}^2} + \frac{2(s_x^2 + s_y^2)}{a_{sx} a_{sy}} \right] \exp\left[-\frac{s_x^2}{2a_{sx}^2} - \frac{s_y^2}{2a_{sy}^2} \right] \tag{2.1}$$

where $s = (s_x, s_y)$ are the source plane coordinates and a_{sx} and a_{sy} are Gaussian source sizes along -x and -y direction. Bottle beam is introduced as difference of two basic Laguerre modes as

$$u_s(s) = u_s(s_x, s_y) = L_{00}(s_x, s_y) - L_{20}(s_x, s_y) \tag{2.2}$$

As it is seen from Eq.2.1, bottle beam expression does not contain any phase term. Intensity profiles of bottle beam for different a_{sx} and a_{sy} Gaussian source sizes are shown below in Fig. 1.
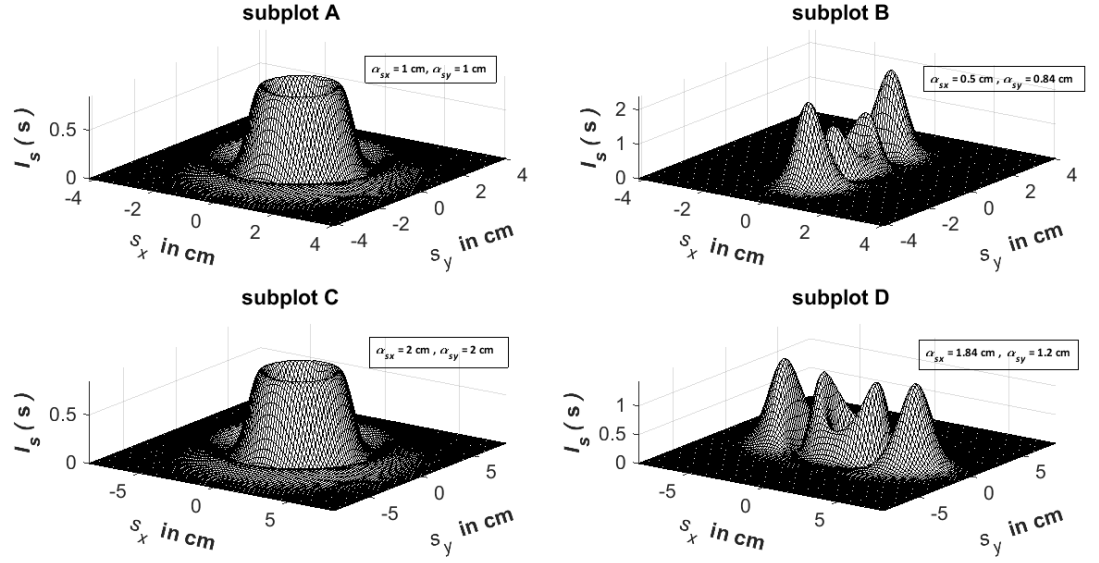
Figure 1 Intensity profile of Bottle beam at source plane for different a_{sx} and a_{sy} Gaussian source sizes

As it is seen from Fig. 1, bottle beams are selected as symmetric when $a_{sx} = a_{sy}$ and asymmetric forms where $a_{sx} \neq a_{sy}$. Symmetric forms of bottle beams are shown in subplots A and C. $\alpha_{sx} = 1$ cm and $\alpha_{sy} = 1$ cm for symmetric small source size beam in subplot A, and $\alpha_{sx} = 2$ cm and $\alpha_{sy} = 2$ cm symmetric large source size beam in subplot C. Symmetric bottle beams have a hallow region on the central on axis and one outer ring. On the other hand, asymmetrical forms of small and large source size beams are generated as in subplot C and subplot D. Equal power identity is considered for the selection of asymmetrical beams. Meaningfully, subplot A and B have the same power and power of subplot C and D are the same. There is a hallow region and two more lobes along the larger Gaussian source size for the asymmetric bottle beams. Subplot B shows asymmetric small source size beam where $\alpha_{sx} = 0.5$ cm and $\alpha_{sy} = 0.84$ cm. In this plot, there is a hallow on the origin and there are two side lobes along $-y$ axis. In subplot D, asymmetric large source size beam is introduced as $\alpha_{sx} = 1.84$ cm and $\alpha_{sy} = 1.2$ cm. Different from subplot B, side lobes are placed alon $-x$ axis since $\alpha_{sx} > \alpha_{sy}$.

In other point of view, orbital angular momentum is the new trend for optical wireless communication. That's why phase distribution of bottle beam is analyzed

for small source size cases. To carry information via topological charge, vortex term $\exp(-jv\phi)$ is added to the source field expression which is defined in Eq. 2.1. Here v denotes the topological charge and ϕ refers to phase angle.

$$u_{s1}(s,n) = u_{s1}(s_x, s_y, n) = \left[\frac{-(s_x^2 + s_y^2)^2}{2a_{sx}^2 a_{sy}^2} + \frac{2(s_x^2 + s_y^2)}{a_{sx} a_{sy}} \right] \exp\left[-\frac{s_x^2}{2a_{sx}^2} - \frac{s_y^2}{2a_{sy}^2} \right] \exp(-jv\phi) \qquad (2.3)$$
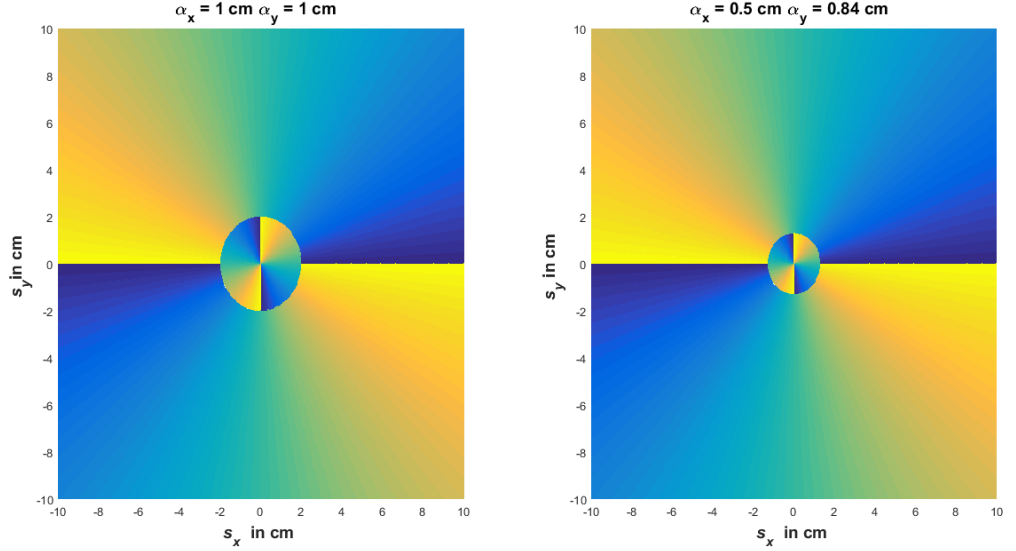
Figure 2 Phase distribution of small source size phase added bottle beams on the source plane.

As it is seen from Fig. 2, radial axial symmetry does not affect the angular phase distribution. While data is loaded to topological charge, changes in the phase pattern is counted. For $v = 2$, there are two phase changes during the anti clockwise motion in the central circle. As compared to the intensity modulation, information is loaded to the phase information of carrier beam.

2.2 Analytical Derivation of Scintillation Expression of Bottle Beam via Rytov Method

Rytov scintillation theory requires free space received field. For this purpose, Huygens-Fresnel integral for free space coordinates is written as

$$u_r\left(r_x,r_y,z=L\right)=\frac{-jk\exp\left(jkL\right)}{4\pi L}\int_{-\infty}^{\infty}\int_{-\infty}^{\infty}ds_x ds_y u_s\left(s_x,s_y,z=0\right)\exp\left\{\frac{jk}{2L}\left[-2s_x r_x-2s_y r_y+s_x^2+s_y^2+r_x^2+r_y^2\right]\right\} \quad (2.4)$$

where $r=\left(r_x,r_y\right)$ are receiver plane coordinates. To see the integral parts clearly, squared terms in Eq. 2.1. must be expanded. Re-organized form of source field expression is obtained as

$$u_s\left(s\right)=u_s\left(s_x,s_y\right)=\left[\frac{\left(s_x^4+s_y^4+2s_x^2 s_y^2+2s_x^2 a_{sx}a_{sy}+2s_y^2 a_{sx}a_{sy}\right)}{2a_{sx}^2 a_{sy}^2}\right]\exp\left[-\frac{s_x^2}{2a_{sx}^2}-\frac{s_y^2}{2a_{sy}^2}\right] \quad (2.5)$$

Eq. 2.5 involves fourth order terms and coupling terms of s_x, s_y, a_{sx}, and a_{sy}. Since Eq. 2.5 involves summation of five terms, this equation must be solved in five parts. For simplicity, we define new variables as $p_x=\frac{L+jka_{sx}^2}{2La_{sx}^2}$, $q_x=\frac{-jkr_x}{2L}$, $p_y=\frac{L+jka_{sy}^2}{2La_{sy}^2}$, and $q_y=\frac{-jkr_y}{2L}$. Then, Huygens-Fresnel integral is organized as

$$u_r\left(r_x,r_y,z=L\right)=\frac{-jk\exp\left(jkL\right)\exp\left(\frac{jk}{2L}\left(r_x^2+r_y^2\right)\right)}{2\pi La_{sx}^2 a_{sy}^2}$$

$$x\int_{-\infty}^{\infty}\int_{-\infty}^{\infty}ds_x ds_y u_{s1}\left(s_x,s_y,z=0\right)\exp\left\{\frac{jk}{2L}\left[-2s_x r_x-2s_y r_y+s_x^2+s_y^2\right]\right\} \quad (2.6)$$

where

$$u_{s1}\left(s_x,s_y,z=0\right)=\left(s_x^4+s_y^4+2s_x^2 s_y^2+2s_x^2 a_{sx}a_{sy}+2s_y^2 a_{sx}a_{sy}\right)\exp\left[-\frac{s_x^2}{2a_{sx}^2}-\frac{s_y^2}{2a_{sy}^2}\right] \quad (2.7)$$

To solve integral that comes from s_x^4 term, integral 3.462.2 from [90] is used. 3.462.2 is written as

$$\int_{-\infty}^{\infty}x^n\exp\left(-px^2+2qx\right)dx=n!\exp\left(\frac{q^2}{p}\right)\sqrt{\frac{\pi}{p}}\left(\frac{q}{p}\right)^n\sum_{k=0}^{\lfloor n/2\rfloor}\frac{1}{(n-2k)!(k)!}\left(\frac{p}{4q^2}\right)^k \quad (2.8)$$

Eq. 2.8 is solved two times for ds_x and ds_y components seperately and it gives

$$I_1 = \int_{-\infty}^{\infty} \int_{-\infty}^{\infty} ds_x ds_y s_x^4 \exp\left[-\frac{s_x^2}{2a_{sx}^2} - \frac{s_y^2}{2a_{sy}^2}\right] \exp\left\{\frac{jk}{2L}\left[-2s_x r_x - 2s_y r_y + s_x^2 + s_y^2\right]\right\}$$

$$= 24\pi \left(\frac{1}{24} + \frac{p_x}{8q_x^2} + \frac{p_x^2}{32q_x^4}\right) \exp\left(\frac{q_x^2}{p_x}\right) \sqrt{\frac{1}{p_x p_y}} \left(\frac{q_x}{p_x}\right)^4 \exp\left(\frac{q_y^2}{p_y}\right) \qquad (2.9)$$

Similarly, integral coming from s_y^4 in Eq. 2.6 and Eq. 2.7 is solved via Eq. 2.8 above and it is written as

$$I_2 = \int_{-\infty}^{\infty} \int_{-\infty}^{\infty} ds_x ds_y s_y^4 \exp\left[-\frac{s_x^2}{2a_{sx}^2} - \frac{s_y^2}{2a_{sy}^2}\right] \exp\left\{\frac{jk}{2L}\left[-2s_x r_x - 2s_y r_y + s_x^2 + s_y^2\right]\right\}$$

$$= 24\pi \left(\frac{1}{24} + \frac{p_y}{8q_y^2} + \frac{p_y^2}{32q_y^4}\right) \exp\left(\frac{q_y^2}{p_y}\right) \sqrt{\frac{1}{p_x p_y}} \left(\frac{q_y}{p_y}\right)^4 \exp\left(\frac{q_x^2}{p_x}\right) \qquad (2.10)$$

It is seen from Eq. 2.9 and Eq. 2.10 that they have $\left(\dfrac{1}{24} + \dfrac{p_{x,y}}{8q_{x,y}^2} + \dfrac{p_{x,y}^2}{32q_{x,y}^4}\right)$ terms

consisting of three parts inside the parenthesis. This causes us extra calculation effort during the evaluation of $H(r, \phi_r, \kappa, \phi_\kappa, \eta)$ function. Next integral coming from coupling term $s_x^2 s_y^2$ is solved via 3.462.8 from the same source [90]. First 3.462.8 is introduced as

$$\int_{-\infty}^{\infty} x^2 \exp\left(-px^2 + 2qx\right) dx = \frac{1}{2p} \exp\left(\frac{q^2}{p}\right) \sqrt{\frac{\pi}{p}} \left(1 + \frac{q^2}{p}\right) \qquad (2.11)$$

Then, integral of coupling term is written and the solution is written as

$$I_3 = 2 \int_{-\infty}^{\infty} \int_{-\infty}^{\infty} ds_x ds_y s_x^2 s_y^2 \exp\left[-\frac{s_x^2}{2a_{sx}^2} - \frac{s_y^2}{2a_{sy}^2}\right] \exp\left\{\frac{jk}{2L}\left[-2s_x r_x - 2s_y r_y + s_x^2 + s_y^2\right]\right\}$$

$$= \frac{\pi}{2p_x p_y} \sqrt{\frac{1}{p_x p_y}} \left(1 + 2\frac{q_x}{p_x}\right)\left(1 + 2\frac{q_y}{p_y}\right) \exp\left(\frac{q_x^2}{p_x}\right) e \exp\left(\frac{q_y^2}{p_y}\right) \qquad (2.12)$$

Next, integral coming from s_x^2 term is written and solved benefiting from 3.462.8 and 3.462.2 as

$$I_4 = 2a_{sx} a_{sy} \int_{-\infty}^{\infty} \int_{-\infty}^{\infty} ds_x ds_y s_x^2 \exp\left[-\frac{s_x^2}{2a_{sx}^2} - \frac{s_y^2}{2a_{sy}^2}\right] \exp\left\{\frac{jk}{2L}\left[-2s_x r_x - 2s_y r_y + s_x^2 + s_y^2\right]\right\}$$

$$= \frac{a_{sx} a_{sy} \pi}{p_x} \sqrt{\frac{1}{p_x p_y}} \left(1 + 2\frac{q_x}{p_x}\right) \exp\left(\frac{q_x^2}{p_x}\right) e \exp\left(\frac{q_y^2}{p_y}\right) \qquad (2.13)$$

Final part of received field expression is solved similar with Eq. 2.13 and it is written as

$$I_5 = 2a_{sx}a_{sy} \int_{-\infty}^{\infty}\int_{-\infty}^{\infty} ds_x ds_y s_y^2 \exp\left[-\frac{s_x^2}{2a_{sx}^2} - \frac{s_y^2}{2a_{sy}^2}\right]\exp\left\{\frac{jk}{2L}\left[-2s_x r_x - 2s_y r_y + s_x^2 + s_y^2\right]\right\}$$

$$= \frac{a_{sx}a_{sy}\pi}{p_y}\sqrt{\frac{1}{p_x p_y}}\left(1 + 2\frac{q_y}{p_y}\right)\exp\left(\frac{q_x^2}{p_x}\right)e\exp\left(\frac{q_y^2}{p_y}\right) \tag{2.14}$$

Received field expression is simply obtained as

$$u_r\left(r_x, r_y, z = L\right) = \frac{-jk\exp(jkL)\exp\left(\frac{jk}{2L}\left(r_x^2 + r_y^2\right)\right)}{2\pi L a_{sx}^2 a_{sy}^2}\left(I_1 + I_2 + I_3 + I_4 + I_5\right) \tag{2.15}$$

Next step in Rytov scintillation theory is to find $H(r, \phi_r, \kappa, \phi_\kappa, \eta)$ function. It is written in Cartesian coordinates as

$$H\left(r_x, r_y, \kappa, \phi_\kappa, \eta\right) = \frac{k^2\exp\left[jk(L-\eta)\right]}{2\pi(L-\eta)u_r\left(r_x, r_y, z = L\right)}\exp\left[\frac{jk\left(r_x^2 + r_y^2\right)}{2(L-\eta)}\right]$$

$$x\int_{-\infty}^{\infty}\int_{-\infty}^{\infty} dr_{1x}dr_{1y}u_r\left(r_{1x}, r_{1y}, z = \eta\right)\exp\left\{j\kappa\left[r_{1x}\cos(\phi_\kappa) + r_{1y}\sin(\phi_\kappa)\right]\right\}$$

$$x\exp\left[\frac{jk}{2(L-\eta)}\left(r_{1x}^2 + r_{1y}^2 - 2r_x r_{1x} - 2r_y r_{1y}\right)\right] \tag{2.16}$$

Since receiver field has five components $H(r, \phi_r, \kappa, \phi_\kappa, \eta)$ function is calculated five main parts and reorganized form of first part is obtained as below

$$H_1\left(r_x, r_y, \kappa, \phi_\kappa, \eta\right) = 24\pi\sqrt{\frac{1}{p_x p_y}}$$

$$x\int_{-\infty}^{\infty}\int_{-\infty}^{\infty} dr_{1x}dr_{1y}\exp\left\{j\kappa\left[r_{1x}\cos(\phi_\kappa) + r_{1y}\sin(\phi_\kappa)\right]\right\}$$

$$x\exp\left[\frac{2jkL(L-\eta) + 2jkL^2 - k^2(L-\eta)}{4L^2(L-\eta)p_x}\left(r_{1x}^2 - 2r_x r_{1x}\right)\right] \tag{2.17}$$

$$x\exp\left[\frac{2jkL(L-\eta) + 2jkL^2 - k^2(L-\eta)}{4L^2(L-\eta)p_y}\left(r_{1y}^2 - 2r_y r_{1y}\right)\right]$$

$$x\left(\frac{k^4 r_{1x}^4}{384L^4 p_x^4} - \frac{k^4 r_{1x}^2}{32L^2 k^2 p_x^3} + \frac{1}{32p_x^2}\right)$$

Eq. 2.17 is solved benefitting 3.462.2 and 3462.8 and written as

14

$$H_1\left(r_x, r_y, \kappa, \phi_\kappa, \eta\right) =$$

$$\sqrt{\frac{1}{p_x p_y r_x r_y}} \exp\left(\frac{\left(r_y \sin(\phi_\kappa) + r_x \cos(\phi_\kappa)\right)\left(p_y\left(2jkL(L-\eta) + 2jkL^2 - k^2(L-\eta)\right)\right)^2}{4L^2(L-\eta)p_x p_y \cos(\phi_\kappa)\sin(\phi_\kappa)}\right)$$

$$x \frac{4L^2(L-\eta)p_y}{\left(2jkL(L-\eta)+2jkL^2-k^2(L-\eta)\right)}\left(-\frac{4L^2(L-\eta)p_x \cos(\phi_\kappa)}{p_y r_x \left(2jkL(L-\eta)+2jkL^2-k^2(L-\eta)\right)}\right)^4$$

$$x\left\{
\begin{array}{l}
-\dfrac{3\pi^2 k^4}{2L^4 p_x^2}\left(\begin{array}{l}\dfrac{1}{24} - \dfrac{p_y\left(2jkL(L-\eta)+2jkL^2-k^2(L-\eta)\right)}{32L^2(L-\eta)p_x \cos^2(\phi_\kappa)}\\[2mm]
+\dfrac{1}{2}\left(\dfrac{p_y\left(2jkL(L-\eta)+2jkL^2-k^2(L-\eta)\right)}{32L^2(L-\eta)p_x \cos^2(\phi_\kappa)}\right)^2\end{array}\right)\\[10mm]
-\dfrac{3\pi^2}{4p_x^2}\\[6mm]
+\dfrac{\pi k^4}{1536L^2 k^2 p_x^3}\left(1+\dfrac{\left(2r_x \cos(\phi_\kappa)\left(p_y\left(2jkL(L-\eta)+2jkL^2-k^2(L-\eta)\right)\right)\right)^2}{4L^2(L-\eta)p_x p_y \cos(\phi_\kappa)}\right)
\end{array}\right\} \quad (2.18)$$

Similarly, second integral involves I_2 and it is calculated using the same equations in [90]. $H_2(r, \phi_r, \kappa, \phi_\kappa, \eta)$ is written in reorganized form as

$$H_2\left(r_x, r_y, \kappa, \phi_\kappa, \eta\right) = 24\pi \sqrt{\frac{1}{p_x p_y}}$$

$$x \int_{-\infty}^{\infty}\int_{-\infty}^{\infty} dr_{1x} dr_{1y} \exp\left\{j\kappa\left[r_{1x}\cos(\phi_\kappa) + r_{1y}\sin(\phi_\kappa)\right]\right\}$$

$$x \exp\left[\frac{2jkL(L-\eta)+2jkL^2-k^2(L-\eta)}{4L^2(L-\eta)p_x}\left(r_{1x}^2 - 2r_x r_{1x}\right)\right] \quad (2.19)$$

$$x \exp\left[\frac{2jkL(L-\eta)+2jkL^2-k^2(L-\eta)}{4L^2(L-\eta)p_y}\left(r_{1y}^2 - 2r_y r_{1y}\right)\right]$$

$$x\left(\frac{k^4 r_{1y}^4}{384L^4 p_y^4} - \frac{k^4 r_{1y}^2}{32L^2 k^2 p_y^3} + \frac{1}{32p_y^2}\right)$$

Then the solution is evaluated as below.

$$H_2\left(r_x, r_y, \kappa, \phi_\kappa, \eta\right) =$$

$$\sqrt{\frac{1}{p_x p_y r_x r_y}} \exp\left(\frac{\left(r_y \sin\left(\phi_\kappa\right) + r_x \cos\left(\phi_\kappa\right)\right)\left(p_y\left(2jkL(L-\eta) + 2jkL^2 - k^2(L-\eta)\right)\right)^2}{4L^2(L-\eta)p_x p_y \cos\left(\phi_\kappa\right)\sin\left(\phi_\kappa\right)}\right)$$

$$x \frac{4L^2(L-\eta)p_y}{\left(2jkL(L-\eta) + 2jkL^2 - k^2(L-\eta)\right)}\left(-\frac{4L^2(L-\eta)p_x \cos\left(\phi_\kappa\right)}{p_y r_x\left(2jkL(L-\eta) + 2jkL^2 - k^2(L-\eta)\right)}\right)^4 \qquad (2.20)$$

$$x\left\{
\begin{aligned}
&-\frac{3\pi^2 k^4}{2L^4 p_y^2}\left(
\begin{aligned}
&\frac{1}{24} - \frac{p_y\left(2jkL(L-\eta) + 2jkL^2 - k^2(L-\eta)\right)}{32L^2(L-\eta)p_x \cos^2\left(\phi_\kappa\right)} \\
&+\frac{1}{2}\left(\frac{p_y\left(2jkL(L-\eta) + 2jkL^2 - k^2(L-\eta)\right)}{32L^2(L-\eta)p_x \cos^2\left(\phi_\kappa\right)}\right)^2
\end{aligned}
\right) \\
&-\frac{3\pi^2}{4p_y^2} \\
&+\frac{\pi k^4}{1536L^2 k^2 p_y^3}\left(1 + \frac{\left(2r_x \cos\left(\phi_\kappa\right)\left(p_y\left(2jkL(L-\eta) + 2jkL^2 - k^2(L-\eta)\right)\right)\right)^2}{4L^2(L-\eta)p_x p_y \cos\left(\phi_\kappa\right)}\right)
\end{aligned}
\right\}$$

Next part, which includes I_3, is reorganized as

$$H_3\left(r_x, r_y, \kappa, \phi_\kappa, \eta\right) = \frac{-jk\exp\left(jkL\right)}{4La_{sx}^2 a_{sy}^2 p_x p_y}\sqrt{\frac{1}{p_x p_y}}$$

$$x\int_{-\infty}^{\infty}\int_{-\infty}^{\infty} dr_{1x}dr_{1y}\exp\left(\frac{j2kLp_x(L-\eta)}{4L^2 p_x(L-\eta)}\left(r_{1x}^2 + r_{1y}^2\right)\right)$$

$$x\exp\left\{j\frac{4L^2 p_x(L-\eta)\kappa}{4L^2 p_x(L-\eta)}\left[r_{1x}\cos\left(\phi_\kappa\right) + r_{1y}\sin\left(\phi_\kappa\right)\right]\right\} \qquad (2.21)$$

$$x\exp\left[\frac{j2kL^2 p_x}{4L^2 p_x(L-\eta)}\left(r_{1x}^2 + r_{1y}^2 - 2r_x r_{1x} - 2r_y r_{1y}\right)\right]$$

$$x\exp\left(\frac{-k^2(L-\eta)r_{1x}^2}{4L^2 p_x(L-\eta)}\right)e\exp\left(\frac{-k^2(L-\eta)r_{1y}^2}{4L^2 p_y(L-\eta)}\right)$$

$$x\left(1 - \frac{jkr_{1x}}{Lp_x} - \frac{jkr_{1y}}{Lp_y} + -\frac{k^2 r_{1x}r_{1y}}{L^2 p_x p_y}\right)$$

Eq. 2.21 is solved via 3.462.2 and 3.462.6. Definition of 3.462.6 is written as

$$\int\limits_{-\infty}^{\infty} x\exp\left(-px^2+2qx\right)dx = \frac{q}{p}\exp\left(\frac{q^2}{p}\right)\sqrt{\frac{\pi}{p}}\left(1+\frac{2q^2}{p}\right) \tag{2.22}$$

After applying these solutions Eq. 2.21 turns into

$$H_3\left(r_x,r_y,\kappa,\phi_\kappa,\eta\right) = \frac{-jk\exp\left(jkL\right)}{4La_{sx}^2 a_{sy}^2 p_x p_y}\sqrt{\frac{1}{p_x p_y}}$$

$$x\exp\left(-\frac{\left(j2L^2 p_x(L-\eta)\left(\kappa\cos\left(\phi_\kappa\right)-kr_x\right)\right)^2}{4L^2 p_x(L-\eta)\left(2kp_x(L-\eta)\left(L^2+L\right)-k^2(L-\eta)\right)}\right)$$

$$x\sqrt{\frac{4\pi L^2 p_x(L-\eta)}{2kp_x(L-\eta)\left(L^2+L\right)-k^2(L-\eta)}}$$

$$x\exp\left(-\frac{\left(j2L^2 p_y(L-\eta)\left(\kappa\sin\left(\phi_\kappa\right)-kr_y\right)\right)^2}{4L^2 p_y(L-\eta)\left(2kp_y(L-\eta)\left(L^2+L\right)-k^2(L-\eta)\right)}\right) \tag{2.23}$$

$$x\sqrt{\frac{4\pi L^2 p_y(L-\eta)}{2kp_y(L-\eta)\left(L^2+L\right)-k^2(L-\eta)}}$$

$$x\left[\begin{array}{c} 1+j\dfrac{L\left(\kappa\cos\left(\phi_\kappa\right)-kr_x\right)}{\left(p_x\left(L^2+L\right)-k^2(L-\eta)\right)}+j\dfrac{L\left(\kappa\sin\left(\phi_\kappa\right)-kr_y\right)}{\left(p_y\left(L^2+L\right)-k^2(L-\eta)\right)} \\[4mm] -\dfrac{\left(\kappa\cos\left(\phi_\kappa\right)-kr_x\right)\left(\kappa\sin\left(\phi_\kappa\right)-kr_y\right)}{\left(p_x\left(L^2+L\right)-k^2(L-\eta)\right)\left(p_y\left(L^2+L\right)-k^2(L-\eta)\right)} \end{array}\right]$$

$H_4\left(r_x,r_y,\kappa,\phi_\kappa,\eta\right)$ and $H_5\left(r_x,r_y,\kappa,\phi_\kappa,\eta\right)$ are solved benefiting from Eq. 2.19 above and they are written below in Eq. 2.24 and Eq. 2.25.

$$H_4\left(r_x, r_y, \kappa, \phi_\kappa, \eta\right) = \frac{-jk \exp\left(jkL\right)}{2La_{sx}a_{sy}p_x}\sqrt{\frac{1}{p_x p_y}}$$

$$x \exp\left(-\frac{\left(j2L^2 p_x(L-\eta)\left(\kappa\cos\left(\phi_\kappa\right) - kr_x\right)\right)^2}{4L^2 p_x(L-\eta)\left(2kp_x(L-\eta)\left(L^2+L\right) - k^2(L-\eta)\right)}\right)$$

$$x \sqrt{\frac{4\pi L^2 p_x(L-\eta)}{2kp_x(L-\eta)\left(L^2+L\right) - k^2(L-\eta)}} \tag{2.24}$$

$$x \exp\left(-\frac{\left(j2L^2 p_y(L-\eta)\left(\kappa\sin\left(\phi_\kappa\right) - kr_y\right)\right)^2}{4L^2 p_y(L-\eta)\left(2kp_y(L-\eta)\left(L^2+L\right) - k^2(L-\eta)\right)}\right)$$

$$x \sqrt{\frac{4\pi L^2 p_y(L-\eta)}{2kp_y(L-\eta)\left(L^2+L\right) - k^2(L-\eta)}}$$

$$x \left[1 + j\frac{L\left(\kappa\cos\left(\phi_\kappa\right) - kr_x\right)}{\left(p_x\left(L^2+L\right) - k^2(L-\eta)\right)}\right]$$

$$H_5\left(r_x, r_y, \kappa, \phi_\kappa, \eta\right) = \frac{-jk \exp\left(jkL\right)}{2La_{sx}a_{sy}p_x}\sqrt{\frac{1}{p_x p_y}}$$

$$x \exp\left(-\frac{\left(j2L^2 p_x(L-\eta)\left(\kappa\cos\left(\phi_\kappa\right) - kr_x\right)\right)^2}{4L^2 p_x(L-\eta)\left(2kp_x(L-\eta)\left(L^2+L\right) - k^2(L-\eta)\right)}\right)$$

$$x \sqrt{\frac{4\pi L^2 p_x(L-\eta)}{2kp_x(L-\eta)\left(L^2+L\right) - k^2(L-\eta)}} \tag{2.25}$$

$$x \exp\left(-\frac{\left(j2L^2 p_y(L-\eta)\left(\kappa\sin\left(\phi_\kappa\right) - kr_y\right)\right)^2}{4L^2 p_y(L-\eta)\left(2kp_y(L-\eta)\left(L^2+L\right) - k^2(L-\eta)\right)}\right)$$

$$x \sqrt{\frac{4\pi L^2 p_y(L-\eta)}{2kp_y(L-\eta)\left(L^2+L\right) - k^2(L-\eta)}}$$

$$x \left[1 + j\frac{L\left(\kappa\sin\left(\phi_\kappa\right) - kr_y\right)}{\left(p_y\left(L^2+L\right) - k^2(L-\eta)\right)}\right]$$

After all these calculations total expression of $H\left(r, \phi_r, \kappa, \phi_\kappa, \eta\right)$ is obtained as

$$H\left(r_x, r_y, \kappa, \phi_\kappa, \eta\right) = \frac{k^2 \exp\left[jk(L-\eta)\right]}{2\pi(L-\eta)u_r\left(r_x, r_y, z=L\right)}\exp\left[\frac{jk\left(r_x^2 + r_y^2\right)}{2(L-\eta)}\right]$$

$$x\left[H_1 + H_2 + H_3 + H_4 + H_5\right] \tag{2.26}$$

18

Finally, scintillation index formulation via Rytov scintillation theory is

$$m^2\left(r,\phi_r,L\right) = 4\pi \int\limits_0^L d\eta \int\limits_0^\infty \kappa\, d\kappa \int\limits_0^{2\pi} d\phi_\kappa$$

$$\mathrm{Re}\begin{bmatrix} H\left(r,\phi_r,\kappa,\phi_\kappa,\eta\right) H^*\left(r,\phi_r,\kappa,\phi_\kappa,\eta\right) \\ +H\left(r,\phi_r,\kappa,\phi_\kappa,\eta\right) H\left(r,\phi_r,-\kappa,\phi_\kappa,\eta\right) \end{bmatrix} \Phi_n\left(\kappa\right) \qquad (2.27)$$

where $\Phi_n\left(\kappa\right) = 0.033 C_n^2 \exp\left[-\kappa^2 \left(\ell_0 / 5.92\right)^2\right] / \left[\kappa^2 + \left(2\pi / L_0\right)^2\right]^{11/6}$, C_n^2 refers to structure constant which defines the strength of turbulence, κ is being the spatial frequency, ℓ_0 is inner scale, and L_0 is the outer scale. Scintillation index is evaluated in two parts since there is a summation expression in Eq. 2.27. Because, it is too complicated to evaluate, numerical simulation using multi hop propagation model (random phase screen) which is explained in chapter 3 is used. Results of MATLAB simulations is shown in chapter 5 and 6 scintillation and BER analysis part of this thesis.

2.3 Source Field Distribution of Sine Hollow Beam

Source field expression of sine hollow beam is taken from [23] as

$$u_s\left(\mathbf{s}\right) = u_s\left(s_x, s_y\right) = \sin^n\left(\frac{s_x^2}{a\alpha_s^2} + \frac{s_y^2}{b\alpha_s^2}\right)\exp\left[-\frac{s_x^2 + s_y^2}{\alpha_s^2}\right] \tag{2.28}$$

where α_s is the Gaussian source size, a and b are beam asymmetry paramaters, and n refers to beam order. Bearing in mind this formula, source intensity distribution of sine hollow beam is plotted as in Fig. 3.
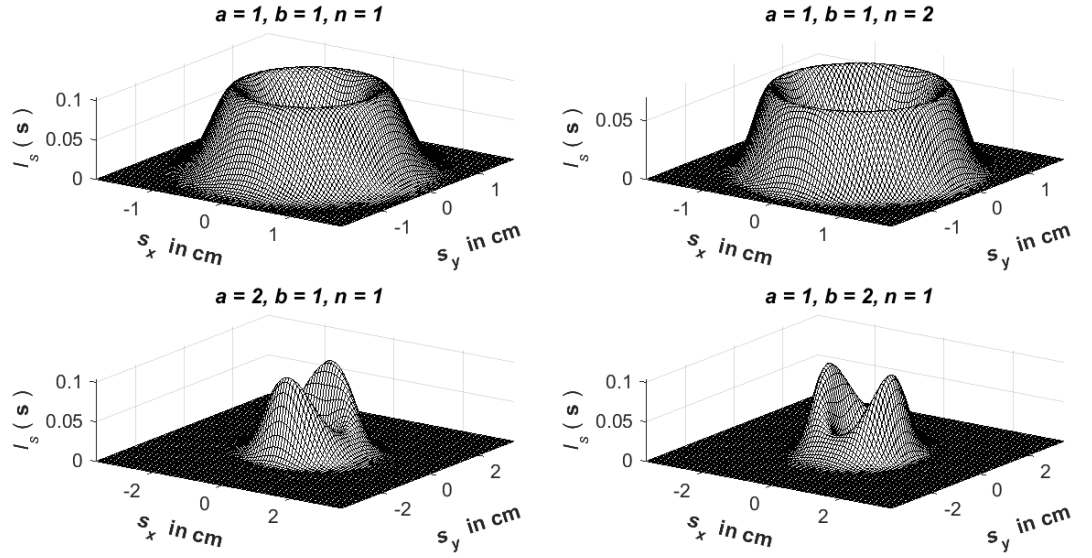
Figure 3 Source intensity distribution of sine hollow beam

As it is shown in Fig. 3, normal sine hollow beams ($a = b$) are placed in first row and anomalous forms ($a \neq b$) are shown in second row. Normal sine hollow beams have a circular view and there is a hollow in the center. This type of beam possesses a thin outer ring where the sharpness increase with rising in order. In case of anomalous beam, intensity distribution of beam looks like a bird bill shape. This shape lies along s_x axis when $a > b$ and rotates ninety degrees if $a < b$.

2.4 Scintillation Expression of Spherical Wave

This part of the thesis involves scintillation expression of spherical wave which is taken from [28]. This analytical formula will be used in comparison of simulation

results in chapters 5. Scintillation expression of spherical wave for strong turbulence region is written as

$$\sigma_I(L) = \exp\left(\frac{0.49\beta_0^2}{\left(1+0.56(1+\theta)\beta_0^{12/5}\right)^{7/6}} + \frac{0.51\beta_0^2}{\left(1+0.69\beta_0^{12/5}\right)^{5/6}}\right) - 1 \qquad (2.29)$$

and θ is the source beam parameter and $\beta_0^2 = 0.4\sigma_R^2$, and $\sigma_R^2 = 1.23C_n^2 k^{7/6} L^{11/6}$ is the Rytov index. Here k indicates wave number. Eq. 2.29 is used to compare the scintillation index measured by our simulation results. Additionally, we take reference spherical wave to show the accuracy of multi-hop propagation model. In simulation environment point like scintillation index is calculated via well known scintillation index formula

$$m_p^2(r_x, r_y) = \frac{\left\langle I_r^2(r_x, r_y)\right\rangle}{\left\langle I_r(r_x, r_y)\right\rangle^2} - 1 \qquad (2.30)$$

where received intensity is $I_r(r_x, r_y) = u_r(r_x, r_y)u_r^*(r_x, r_y)$ In aperture averaged scintillation case, Eq. 2.29 turns into

$$m_A^2 = \frac{\left\langle P_r^2\right\rangle}{\left\langle P_r\right\rangle^2} - 1 \qquad (2.31)$$

where received power is calculated via received intensity $P_r = \iint I_r(r_x, r_y)dr_x dr_y$.

2.5 Bit Error Rate Expression

In this part of the study, theoretical probability of error equation depending on intensity fluctuation is given from [28] as

$$BER = \frac{1}{2}\int_0^\infty p_1(u)\,\text{erfc}\left(\frac{\langle\text{SNR}\rangle u}{2\sqrt{2}}\right)du \qquad (2.32)$$

where erfc denotes complementary error function, $\langle\ \rangle$ refers to ensemble average, and $p_1(u)$ is the probability density function of intensity fluctuation which is defined in log-normal distribution as

$$p_I(u) = \frac{1}{u m_p \sqrt{2\pi}} \exp\left(-\frac{\left(\ln u + 0.5 m_p^2\right)^2}{2 m_p^2}\right) \tag{2.33}$$

Since scintillation index evaluations is sticked in analytical approach, numerical values are taken from simulation results of 3.3 km distance. Then probability of error values for bottle and sine hollow beams are evaluated and plotted in chapter 5 and 6 respectively. In addition, error counting is applied in optical wireless communication using bottle beam and results are compared with theoretical formula in Eq. 2.32.

2.6 Kurtosis parameter

In this part of the thesis Kurtosis parameter formulation is given benefiting from [37]. Formulations of Kurtosis parameters are given as

$$K_{x4} = \int_{-\infty}^{\infty} \int_{-\infty}^{\infty} r_x^4 \left\langle I\left(r_x, r_y\right)\right\rangle dr_x dr_y \tag{2.34}$$

$$K_{y4} = \int_{-\infty}^{\infty} \int_{-\infty}^{\infty} r_y^4 \left\langle I\left(r_x, r_y\right)\right\rangle dr_x dr_y \tag{2.35}$$

$$K_{x2} = \int_{-\infty}^{\infty} \int_{-\infty}^{\infty} r_x^2 \left\langle I\left(r_x, r_y\right)\right\rangle dr_x dr_y \tag{2.36}$$

$$K_{y2} = \int_{-\infty}^{\infty} \int_{-\infty}^{\infty} r_y^2 \left\langle I\left(r_x, r_y\right)\right\rangle dr_x dr_y \tag{2.37}$$

$$K_{x2y2} = \int_{-\infty}^{\infty} \int_{-\infty}^{\infty} r_x^2 r_y^2 \left\langle I\left(r_x, r_y\right)\right\rangle dr_x dr_y \tag{2.38}$$

$$K_{x0y0} = \int_{-\infty}^{\infty} \int_{-\infty}^{\infty} \left\langle I\left(r_x, r_y\right)\right\rangle dr_x dr_y \tag{2.39}$$

Using Eq. 2.32 to 2.37 above, formulation of main parameter is defined as

$$K = \frac{K_{x4} + 2K_{x2y2} + K_{y4}}{K_{x2} + 2K_{x2}K_{y2} + K_{y2}} K_{x0y0} \tag{2.40}$$

After substituting all Kurtosis parameter equation in to Eq. 2.38 we have

$$K = \frac{\int\limits_{-\infty}^{\infty}\int\limits_{-\infty}^{\infty} \left(r_x^2 + r_y^2\right)^2 \left\langle I\left(r_x, r_y\right)\right\rangle^2 dr_x dr_y}{\int\limits_{-\infty}^{\infty}\int\limits_{-\infty}^{\infty} \left(r_x^2 + r_y^2 + 2r_x^2 r_y^2\right)\left\langle I\left(r_x, r_y\right)\right\rangle dr_x dr_y}$$

(2.41)

CHAPTER 3

MULTI HOP PROPAGATION AND ITS APPLICATION

In this part of study, random phase screen derivations and application to optical bottle beam and sine hollow beam are carried out. First, derivation of random phase screen is analyzed and then simulation settings are determined and an example of pseudo code is given.

3.1 Derivation of RPS

Benefitting from [88], received field after random phase screen approach is written as

$$
\begin{aligned}
u_r(r,L) &= \frac{-jk\exp(jkL)}{2\pi L}\exp\left[\frac{jk}{2L}\left(\frac{m-1}{m}\right)r^2\right]\exp\left[\theta(r)\right]u_{s2}(s)\otimes h(s) \\
&= \frac{-jk\exp(jkL)}{2\pi L}\exp\left[\frac{jk}{2L}\left(\frac{m_f-1}{m}\right)r^2\right]\exp\left[\theta(\mathbf{r})\right]\int_{-\infty}^{\infty}\int_{-\infty}^{\infty}d^2s\,u_{s2}(s)\exp\left[\frac{jk}{2Lm_f}(r-ms)^2\right]
\end{aligned}
\tag{3.1}
$$

where $r = ms$. Here m refers to magnification factor determining the amount of diffraction and spreading effects. Additionally,

$$
u_{s2}(\mathbf{s}) = u_s(s)\exp\left[\frac{jk}{2L}\left(1-m_f\right)s^2\right]
\tag{3.2}
$$

For $u_s(s)$, we substitute the source field expression of bottle beam and reorganize the received field as

24

$$u_r(r,L) = \frac{-jk \exp(jkL)}{2\pi L} \exp\left[\frac{jk}{2L}\left(\frac{m_f-1}{m_f}\right)r^2\right] \exp\left[\theta(r)\right] u_{s2}(s) \otimes h(s)$$

$$= \frac{-jk \exp(jkL)}{2\pi L} \exp\left[\frac{jk}{2L}\left(\frac{m_f-1}{m_f}\right)r^2\right] \exp\left[\theta(r)\right] \int_{-\infty}^{\infty}\int_{-\infty}^{\infty} d^2s \left[\frac{-s^4}{32\alpha^4}+\frac{2s^2}{\alpha^2}\right] \qquad (3.3)$$

$$x\exp\left[-\frac{s^2}{64\alpha^3}\right] \exp\left[\frac{jk}{2Lm_f}(r-m_f s)^2\right] \exp\left[\frac{jk}{2L}(1-m_f)s^2\right]$$

Since Eq. 4.3 is too complicated to evaluate, it is numerically calculated in MATLAB.

3.2 Simulation Settings

In the simulation part of this thesis, we started $s_{x1}=10\,\text{cm}\,X\,s_{y1}=10\,\text{cm}$ source plane settings for both symmetric and asymmetric small source size bottle beams and Gaussian beam as it is shown in subplot A in Fig. 4. Source plane dimension are extended to $s_{x2}=40\,\text{cm}\,X\,s_{y2}=40\,\text{cm}$ for both large source size bottle beams to cover the footprint of the beam and it is shown in subplot B in Fig. 4. All beams are generated using 512 X 512 grid view. Since commercial systems use circular lenses, small source plane corresponds to transmitter lens with radius $r_{t1}=5.6\,cm$ which is shown in subplot C in Fig. 4 below. Large source plane is equal to transmitter lens with radius $r_{t2}=22.5\,cm$ in commercial systems having rectangular shape with coordinates s_{x3} and s_{y3} as it is seen in subplot D in Fig. 4. Grid spacing is determined for each case as $d1=\frac{10}{512},\frac{40}{512}$. Operating wavelength is chosen as $\lambda=1550\,nm$. Then, propagation is performed via multi hop propagation model which is shown in Fig. 5. 21, 51, and 91 randomly generated screens are placed to the distances of 0-1200m, 1200-3200m, and 3200-5600m between transmitter and receiver in order to increase the accuracy of the model.

Figure 4 Transmitter grid and eqivalent circular view
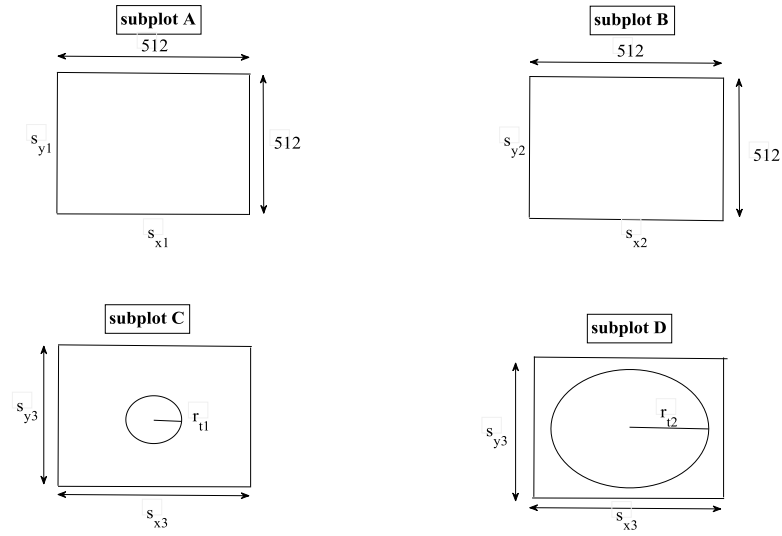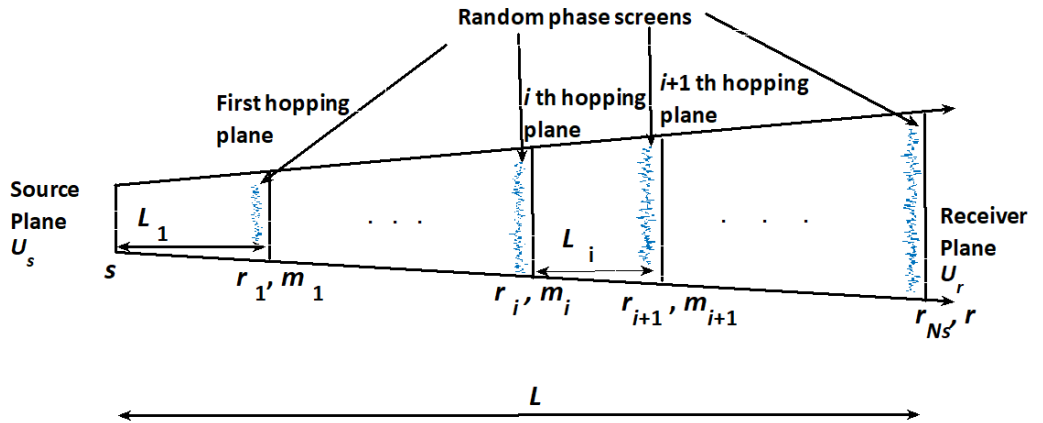

Figure 5 Multi hop propagation model

Along the propagation axis magnification must be applied since diffraction and spreading effects of turbulence. Magnification factor is defined as

$$m = \prod_{i=1}^{N_s} m_i \tag{3.4}$$

where m is total magnification factor, m_i refers to magnification factor of each phase screen, and N_s refers to total number of screens.
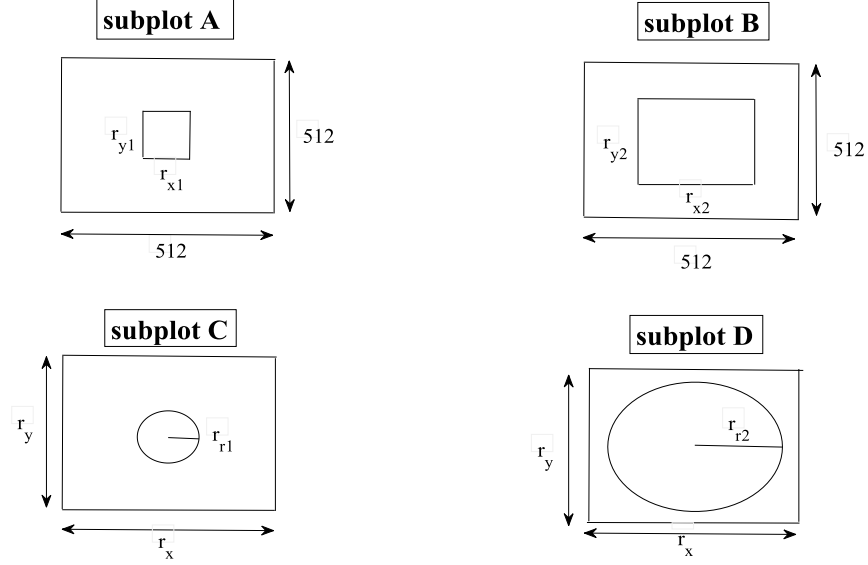
Figure 6 Receiver aperture grid and equivalent circular view

For intensity profile, phase profile, Kurtosis parameter, and scintillation analysis, we carried out simulations 500 times to satisfy averaging. Source power of all beams are set to unity for scintillation comparison. To apply aperture averaged scintillation, receiver openings are set as $r_{x1} = 80 \; X \; r_{y1} = 80$ and $r_{x2} = 180 \; X \; r_{y2} = 180$ grids which correspond to circular aperture with radius $r_{r1} = 42 \; cm$ and $r_{r2} = 95 \; cm$. At this point, point-like scintillation becomes aperture average scintillation if $r_r > \sqrt{0.5\lambda L/\lambda}$ [52]. Receiver aperture grid and circular views are shown in Fig. 6 above. During the probability of error and signal to noise ratio analysis, we determine source powers of all beams to 21.1mW to set the initial conditions the same. 2-ASK is used as modulation type. Link distance is set as 3.3km. Then, we apply error counting principle over 100000 bits. Transmitted and received bits are compared at the receiver side and number of bits with error are divided into total number of bits. Then signal to noise ratio is taken from [48] as

$$\text{SNR} = \frac{\text{signal power}}{\text{noise power}} = \frac{P_r}{\sigma_{SN}^2 + \sigma_{TN}^2 + \sigma_{SC}^2} \tag{3.5}$$

where σ_{SN}^2 refers to variance of shot noise, σ_{TN}^2 variance of thermal noise, and. While designing the simulation set up four main constraints must be taken into account [91]. These constraints are listed as

27

a) Grid interval in transverse plane Δ_s must be less than Fresnel distance for each propagation distance $L_{Fr}(L_i)$.

b) We must set Rytov index of each propagation step $\sigma_R^2(L_i)$ to max %10 of Rytov index of total propagation $\sigma_R^2(L)$.

c) Eq. 4.6 must be satisfied.

$$L_{Fr}(L_i) < \Delta_s \sqrt{N_s N_{ss}} \tag{3.6}$$

where N_{ss} is split-step number and N_s grid size which is taken as 512 in our study.

d) We must set scintillation index less than 0.1.

L_i propagation step distance is checked whether Fried parameter is less than 0.1 for weak turbulent regime or not $(r_0 < 0.1)$. Fried parameter also known is defined in [33] as

$$r_0 = \left(0.423 \mathrm{k}^2 \int_0^{L_i} C_n^2(L) \left(\frac{L}{L_i} \right)^{5/3} dL \right)^{-3/5} \tag{3.7}$$

Phase screens are generated benefiting from phase power spectral density which is defined as

$$\Phi_\phi(\kappa) = 0.49 \mathrm{r}_0^{-5/3} \frac{\exp\left(-\kappa^2 / \kappa_m^2\right)}{\left(\kappa^2 / \kappa_0^2\right)^{11/6}} \tag{3.8}$$

where $\kappa_m = 5.92\ell_0$ and $\kappa_0 = 2\pi/L_0$. Based on above information example psuedo code for propagation and calculation of Kurtosis parameter is given below.

Initialization of variables
Souce plane settings
Source beam generation

FOR distance of each hop

Rytov variance calculation

Setting for screen properties

Constraints check

FOR number of realization

Screen generation

Turbulence propagation

Receiver plane coordinates

Received field and intensity measurements

Calculation of Kurtotsis Parameter

ENDFOR

ENDFOR

Moreover, an example psuedo code for BER and SNR measurement is given as

Initialization of variables

Souce plane settings

Source beam generation

FOR number of transmitted bits

Rytov variance calculation

Setting for screen properties

Constraints check

Screen generation

Turbulence propagation

Receiver plane coordinates

Photodiode settings

Received power measurement and detection

ENDFOR

Comparison of transmitted and received bits

SNR evaluation

CHAPTER 4

PROPAGATION PROPERTIES OF BOTTLE BEAM

In this part of the thesis, intensity profiles of selected bottle beam with selected settings and are analyzed. Kurtosis parameter of selected bottle beams are compared with Gaussian beam [92]. In another point of view, vortex term is added to bottle beam source expression then it is tested whether this type of beam is suitable with carrying information via topological charge.

4.1 Intensity Profile Analysis of Small Source Size Symmetric Bottle Beam

Fig. 7 and 8 show intensity profiles of bottle beam when $\alpha_{sx} = 1\,\text{cm}$ and $\alpha_{sy} = 1\,\text{cm}$ in subplot A of Fig. 1 through propagation.
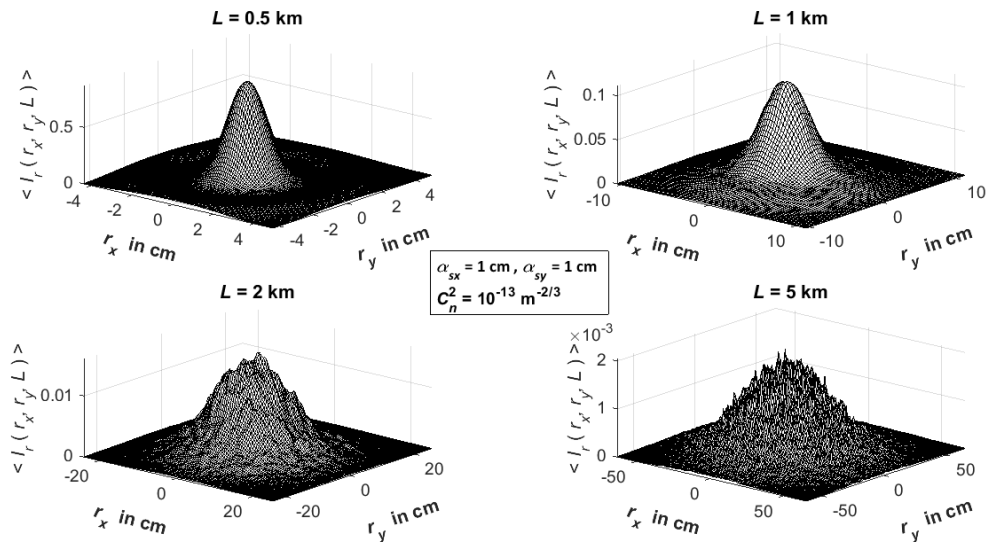

Figure 7 Intensity distribution of bottle beam with source settings $\alpha_{sx} = 1\,\text{cm}$ and $\alpha_{sy} = 1\,\text{cm}$ when $C_n^2 = 10^{-13}\,\text{m}^{-2/3}$.

Fig. 7 shows the intensity distribution of bottle beams along the propagation axis. On the source plane source size dimensions set as $\alpha_{sx} = 1\,\text{cm}$ and $\alpha_{sy} = 1\,\text{cm}$. As it is seen from the figure, bottle beam view turns into a Gaussian shape after 500 m propagation. Outer ring of bottle beam vanishes after 1 km distance and it joins to the central lobe. Affect of turbulence is seen after 2 km propagation. As it is seen from the dimensions of receiver plane, beam spreads along the propagation axis.

Figure 8 Intensity distribution of bottle beam with source settings $\alpha_{sx} = 1\,\text{cm}$ and $\alpha_{sy} = 1\,\text{cm}$ when $C_n^2 = 10^{-14}\,\text{m}^{-2/3}$.

Fig. 8 illustrates the intensity distribution of bottle beams having the source settings $\alpha_{sx} = 1\,\text{cm}$ and $\alpha_{sy} = 1\,\text{cm}$ when $C_n^2 = 10^{-14}\,\text{m}^{-2/3}$. As compared to previous figure, outer ring of bottle beam survives until 5km propagation distance. On the other hand, bottle beam again turns into Gaussian beam after 500 m link distance. Since turbulence is less, bottle beam protects its outer ring even in 5km distance. Looking at the receiver plane dimensions, it can be seen that beams spreads less as compared to previous figure because turbulence is also less.

4.2 Intensity Profile Analysis of Small Source Size Asymmetric Bottle Beam

In this section, Fig. 9 and 10 present intensity distribution of bottle beam which has $\alpha_{\text{sx}} = 0.5\,\text{cm}$ and $\alpha_{\text{sy}} = 0.84\,\text{cm}$ in subplot B in Fig. 1 along the propagation path.

Figure 9 Intensity distribution of bottle beam with source settings $\alpha_{\text{sx}} = 0.5\,\text{cm}$ and $\alpha_{\text{sy}} = 0.84\,\text{cm}$ when $C_n^2 = 10^{-13}\,\text{m}^{-2/3}$.

Fig. 9 investigates intensity distribution of asymmetric small source size beam with settings $\alpha_{\text{sx}} = 0.5\,\text{cm}$ and $\alpha_{\text{sy}} = 0.84\,\text{cm}$ when $C_n^2 = 10^{-13}\,\text{m}^{-2/3}$ atmospheric condition. As compared to subplot B in Fig. 1, on-axis intensity increases up to 500m propagation and then decreases in 1km distance. Outer lobes of asymmetric beam still survive at 1 km and they nearly vanish at 2 km propagation. In the end of propagation at 5km, asymmetic small source size beam turns into Gaussian shape. Beam size increases as it is observed from the receiver plane dimensions.

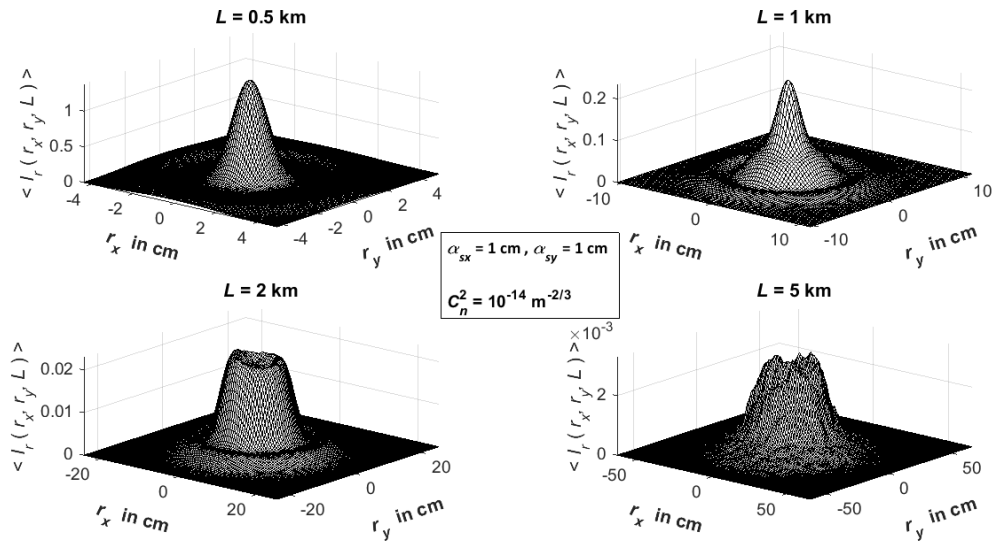**Figure 10** Intensity distribution of bottle beam with source settings $\alpha_{sx} = 0.5$ cm and $\alpha_{sy} = 0.84$ cm when $C_n^2 = 10^{-14}\,\mathrm{m}^{-2/3}$.

Fig. 10 demonstrates the beam evolution of small source size asymmetric bottle beam having $\alpha_{sx} = 0.5$ cm and $\alpha_{sy} = 0.84$ cm under atmospheric conditions of $C_n^2 = 10^{-14}\,\mathrm{m}^{-2/3}$. On axis intensity raises rapidly up to 500 m propagation distance comparing with subplot B in Fig. 1. Then, on axis intensity decreases and asymmetric lobes come closer to each other. In this case, outer asymmetic lobes can be seen at 5 km distance. It is still in the form of asymmetic bottle beam after 5 km progation. As a result of this section, we investigate that asymmetric bottle beams survives more compared to their corresponding symmetric ones.

4.3 Intensity Profile Analysis of Large Source Size Symmetric Bottle Beam

We show intensity distribution of bottle beam when $\alpha_{sx} = 2$ cm and $\alpha_{sy} = 2$ cm in subplot C of Fig.1 along propagation path in this section.
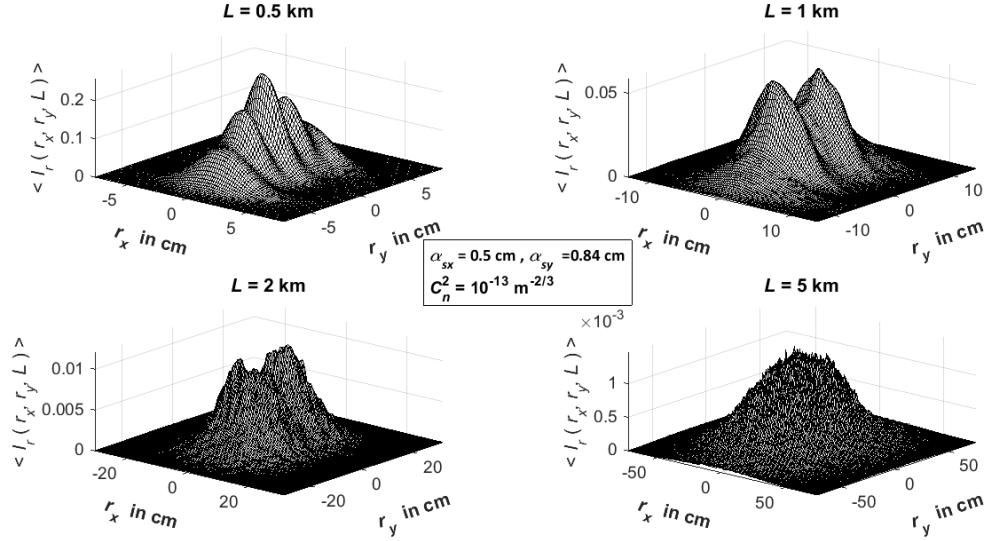

Figure 11 Intensity distribution of bottle beam with source settings $\alpha_{sx} = 2$ cm and $\alpha_{sy} = 2$ cm when $C_n^2 = 10^{-13} \text{m}^{-2/3}$.

Fig. 11 shows how large source size symmetric bottle beam with settings $\alpha_{sx} = 2$ cm and $\alpha_{sy} = 2$ cm changes when structure constant $C_n^2 = 10^{-13} \text{m}^{-2/3}$. As it is seen from figure above, on axis intensity slowly increases up to 500 m distance when source beam is taken as subplot C in Fig. 1. Then, outer ring of bottle beam joins to the on axis main intensity after 1 km propagation. After that distance, large source size symmetric bottle beam turns into Gausian beam.
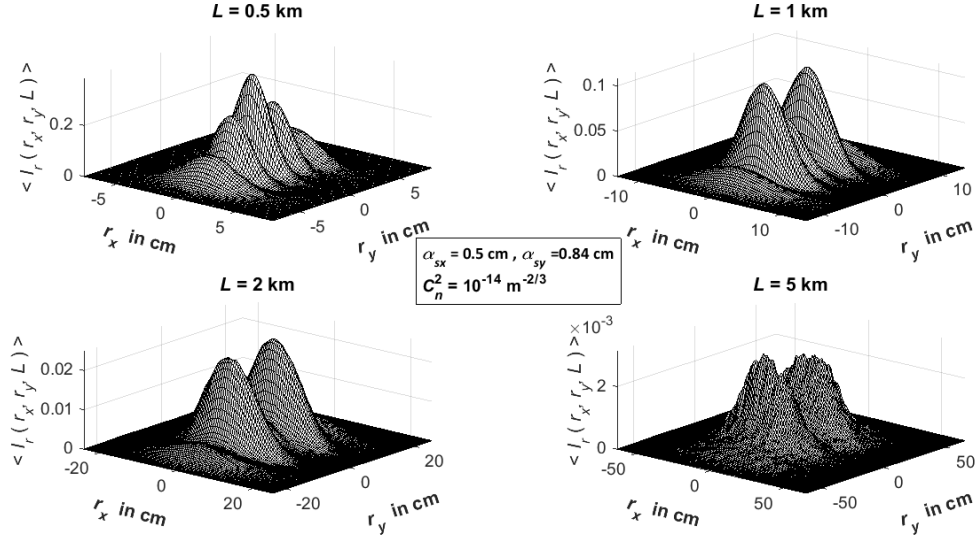
Figure 12 Intensity distribution of bottle beam with source settings $\alpha_{sx} = 2$ cm and $\alpha_{sy} = 2$ cm when $C_n^2 = 10^{-14} \text{m}^{-2/3}$.

It is easier to see beam evolution of large source size symmetric bottle beam when $\alpha_{sx} = 2$ cm and $\alpha_{sy} = 2$ cm while $C_n^2 = 10^{-14} \text{m}^{-2/3}$ in Fig. 12. Comparing with subplot C in Fig. 1 and Fig. 12, it is seen that on axis intensity increases rapidly and hallow region vanishes up to 500m distance. Outer ring survives until 5 km distance. Finally, bottle beam turns into gaussian shape. It is observed that beam spreading is less as compared to previous figure since turbulence is less.

4.4 Intensity Profile Analysis of Large Source Size Asymmetric Bottle Beam

Intensity profiles of bottle beam when $\alpha_{sx} = 1.84$ cm and $\alpha_{sy} = 1.2$ cm which is showed in subplot D of Fig. 1 is analyzed in this section for different turbulence conditions.
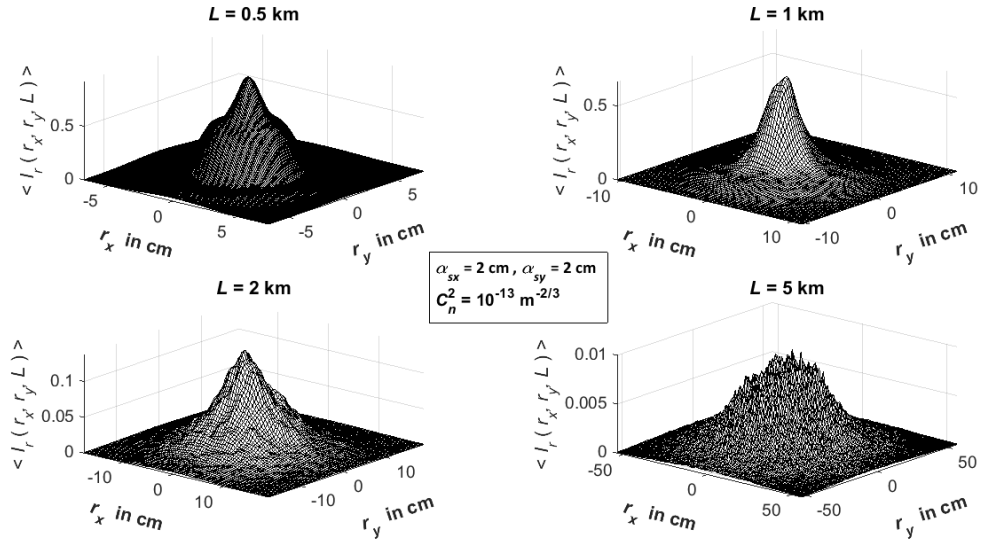

Figure 13 Intensity distribution of bottle beam with source settings $\alpha_{sx} = 1.84$ cm and $\alpha_{sy} = 1.2$ cm when $C_n^2 = 10^{-13}$ m$^{-2/3}$.

As it is seen from Fig. 13 asymmetric large source size beam which has $\alpha_{sx} = 1.84$ cm and $\alpha_{sy} = 1.2$ cm evolves under turbulent conditions when $C_n^2 = 10^{-13}$ m$^{-2/3}$. It can be seen that on axis intensity raises rapidly however there is a hallow region on the source plane in subplot D of Fig. 1. Asymmetircal lobes combine with the on axis intensity at 2 km distance. As it is compared with Fig. 9, this type of beam quickly turns into Gaussian shape as compared to small source size asymmetric beam under the same atmospheric conditions.

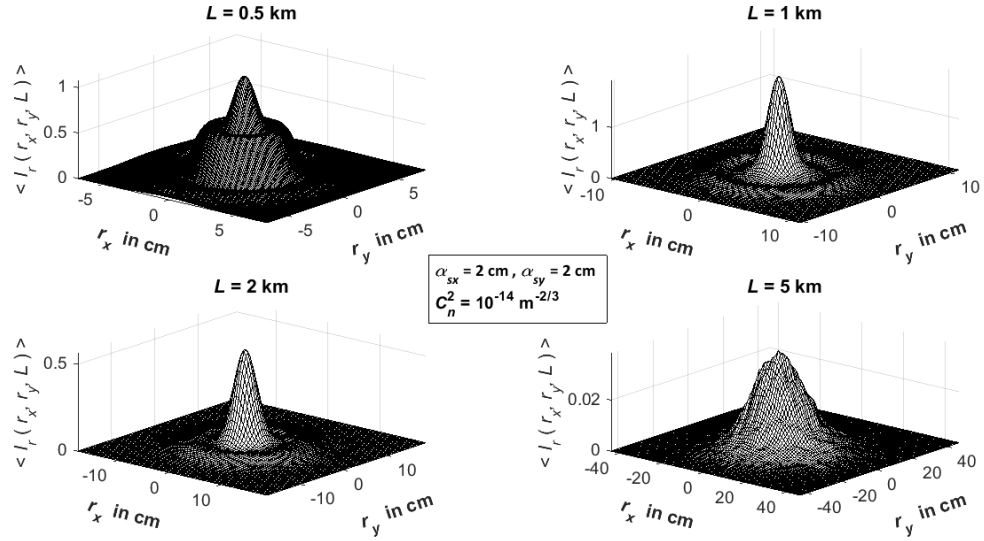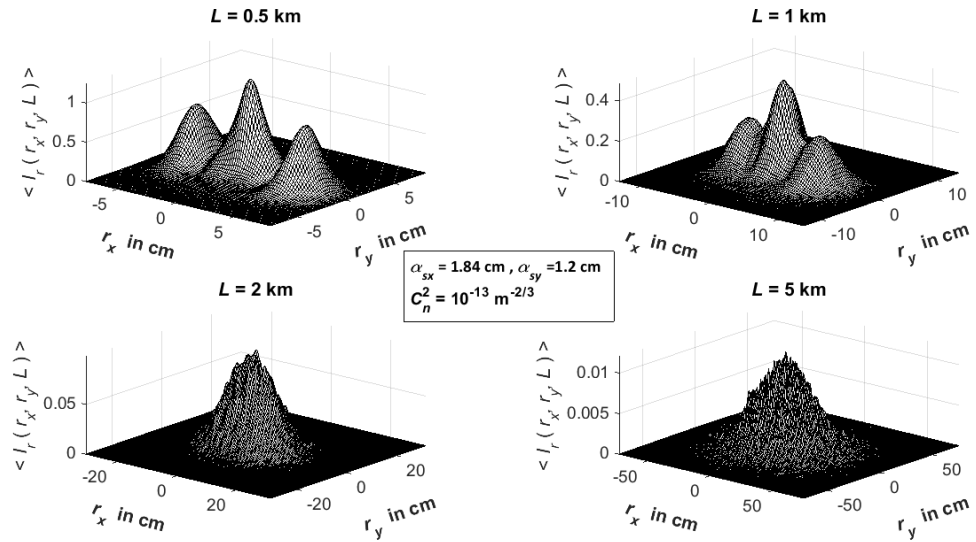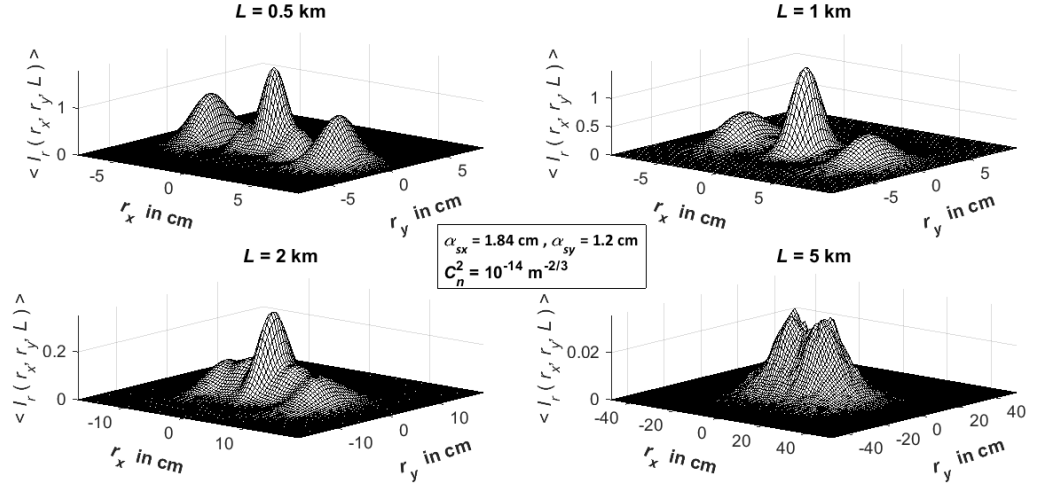**Figure 14** Intensity distribution of bottle beam with source settings $\alpha_{sx} = 1.84$ cm and $\alpha_{sy} = 1.2$ cm when $C_n^2 = 10^{-14}\,\text{m}^{-2/3}$.

As it is similar with previous figure Fig. 13, firstly on axis intensity of asymmetric bottle beam when $\alpha_{sx} = 1.84$ cm and $\alpha_{sy} = 1.2$ cm raises quickly during the beam evolution along propagation path. Then outer asymmetric parts come together and creates nearly Gaussisan shape. Evolution of asymmetric large source size beam occurs faster as compared to asymmetric small source size beam as it is seen from Fig. 10. As a results of intesity profiles, both asymmetric beams protects their shape more than their corresponding symmetric forms along the propagation axis. This observation is valid for both $C_n^2 = 10^{-13}\,\text{m}^{-2/3}$ and $C_n^2 = 10^{-14}\,\text{m}^{-2/3}$.

Consequently, intensity profiles along the propagation axis emphesize that asymmetric forms of both small and large source size beams preserve their shape as compared to corresponding symmetric forms. Between small and large source size beams having the same symmetric property, large source size beams turn into Gaussian beam quicker underneath the same atmospheric condition. In physical point of view, these investigations can be lead to asymmetric bottle beams will have less scintillation.

4.5 Kurtosis Parameter Analysis of Bottle Beam

Fig. 15 shows the Kurtosis parameter variations of selected bottle beams and Gaussian beam when structure constant $C_n^2 = 10^{-13}\,\mathrm{m}^{-2/3}$. Gaussian beam is shown as GB in all remainig plots of kurtosis parameter, scintillation, and BER analysis parts. All beams has increasing behaviour up to some distance then they they show decaying performance. As it is seen from Fig. 11 and Fig. 13, large source size beams have a smooth intensity profiles up to 1 km and then they lose their sharpness. Fig. 11 indicates that symmetric large source size beams loses its sharpness after 1 km and asymmetric large source size beam loses its sharpness after 1.5 km distance. On the other hand, small source size beams have clear view up to 1 km and then their intensity profiles become dirty. Among all selected beams, symmetric large source size bottle beam with $\alpha_{sx} = 2$ cm and $\alpha_{sy} = 2$ cm has the best Kurtosis parameter. Beam with $\alpha_{sx} = 1.84$ cm and $\alpha_{sy} = 1.2$ cm is still better than Gaussian beam. Finally, both small source size bottle beams have the worst performance in terms of Kurtosis parameter.

Fig. 16 indicates the Kurtosis parameter behavior of all selected bottle beams and comparison with Gaussian beam underneath $C_n^2 = 10^{-14}\,\mathrm{m}^{-2/3}$. All beams have raising behaviour in closer distances and then all of them show stable performance. Among all those beams, symmetric large source size beam has the best performance meaning that this beam has the most clear intensity profile. Asymmetric large source size beam is also better than Gaussian beam in longer distances. Finally, both small source size beams have the worst performance in terms of Kurtosis parameter. It means that sharpness of their intensity profile is the least among the others.
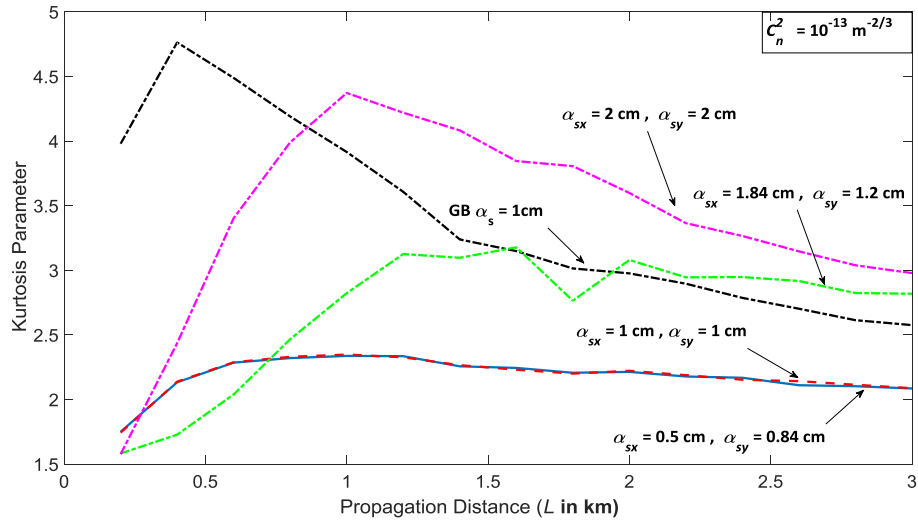
Figure 15 Kurtosis parameter variations of selected bottle beams and Gaussian beam when $C_n^2 = 10^{-13} \text{m}^{-2/3}$.
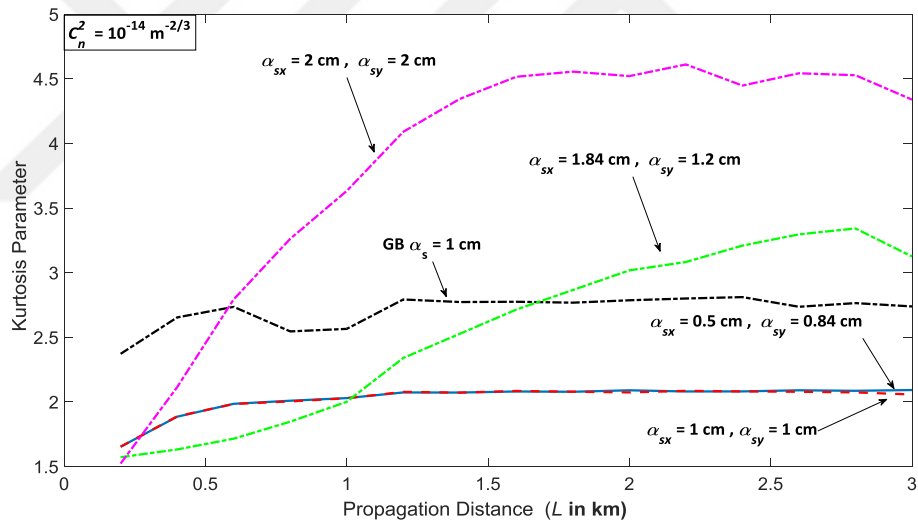
Figure 16 Kurtosis parameter variations of selected bottle beams and Gaussian beam when $C_n^2 = 10^{-14} \text{m}^{-2/3}$.

4.6 Phase Distribution of Small Source Size Symmetric Bottle Beam

This part involves phase distribution of vortexity added symmetric small source size bottle beam which has $\alpha_{sx} = 1\,\text{cm}$ and $\alpha_{sy} = 1\,\text{cm}$ along the propagation path where $v = 2$ in Eq. 2.3. Main idea in this section is carry information via topological charge.

Figure 17 Phase distribution of bottle beam with source settings $\alpha_{sx} = 1\,\text{cm}$ and $\alpha_{sy} = 1\,\text{cm}$ when $C_n^2 = 10^{-13}\,\text{m}^{-2/3}$.

Fig. 17 shows the phase distribution of vortex added bottle beam with $\alpha_{sx} = 1\,\text{cm}$ and $\alpha_{sy} = 1\,\text{cm}$ for $C_n^2 = 10^{-13}\,\text{m}^{-2/3}$. It is seen from Fig. 17 that phase information is vanishes for more than 2 km link distances. However phase information can be identified up to 2 km distance, phase detection can be applied 1 km communication distance.

Fig. 18 displays the phase distribution of vortex added bottle beam with $\alpha_{sx} = 1\,\text{cm}$ and $\alpha_{sy} = 1\,\text{cm}$ for $C_n^2 = 10^{-14}\,\text{m}^{-2/3}$. Phase distribution is more clear since strengh of turbulence reduces. Clear communication link using topological charge can be established more than 2 km distance because phase information can be

read up to that distance. Moreover, communication up to 5 km can be satisfied if sensitive phase detectors are used.

Figure 18 Phase distribution of bottle beam with source settings $\alpha_{\mathrm{sx}} = 1\,\mathrm{cm}$ and

$$\alpha_{\mathrm{sy}} = 1\,\mathrm{cm}\ \text{when}\ C_n^2 = 10^{-14}\,\mathrm{m}^{-2/3}\ .$$

4.7 Phase Distribution of Small Source Size Asymmetric Bottle Beam

In this part of the thesis phase distribution of vortex added asymmetric small source size bottle beam which has $\alpha_{\mathrm{sx}} = 0.5\,\mathrm{cm}$ and $\alpha_{\mathrm{sy}} = 0.84\,\mathrm{cm}$ is examined.

Fig. 19 investigates that optical wireless communication link utilizing topological charge can be established up to 500 m link distance. Then phase information on the center mixes and demodulation will be unsuccesful. Even though, additional phase information coming from additional modes can be read up to 2 km distance, demodulation will be inefficient for these distances. As it is seen from the figure, phase information vanishes at 5km distance.

Fig. 20 shows phase behaviour of vortex added asymmetric bottle beam under moderate turbulent region. Information loaded to toplogical charge free space optics communication link can be established over 2 km distance. Although phase information is read up to 5 km distance, it is foreseen that demodulation will be unsuccesful for these distances. As compared to Fig. 18, phase information is less

41

clear than there. To decide on link distance and detect information from topological charge, counter integral must be evaluated. Our investigations on Fig. 17 to 20 is done via eye inspection.

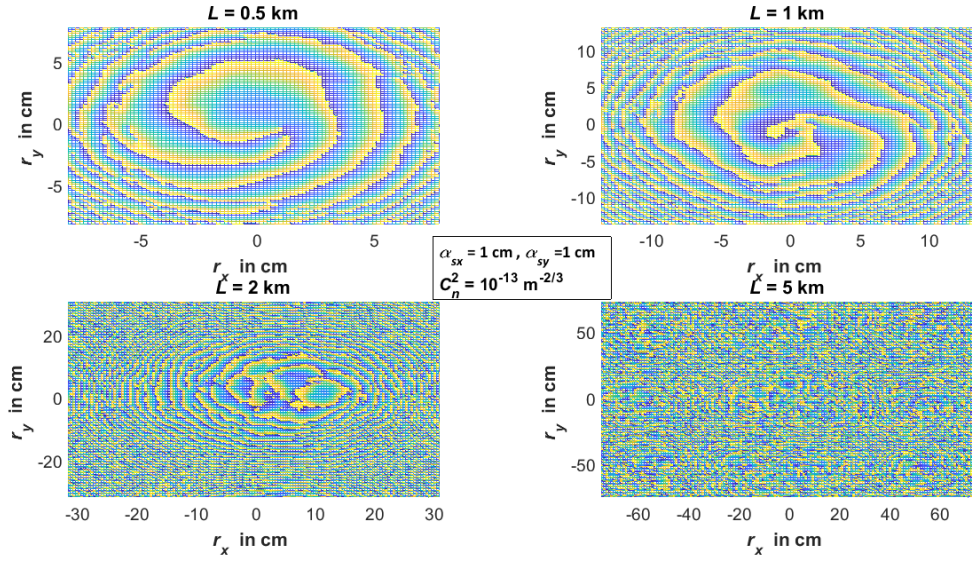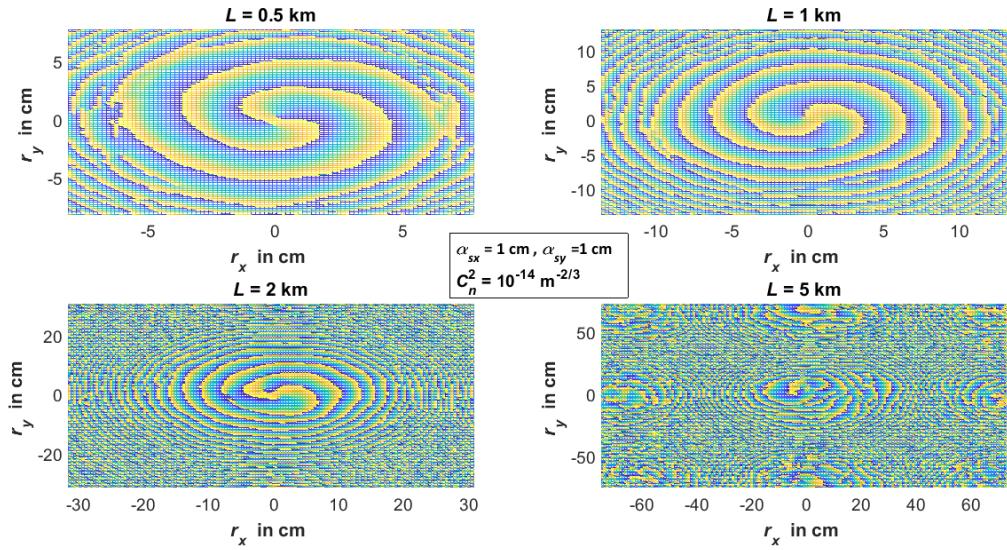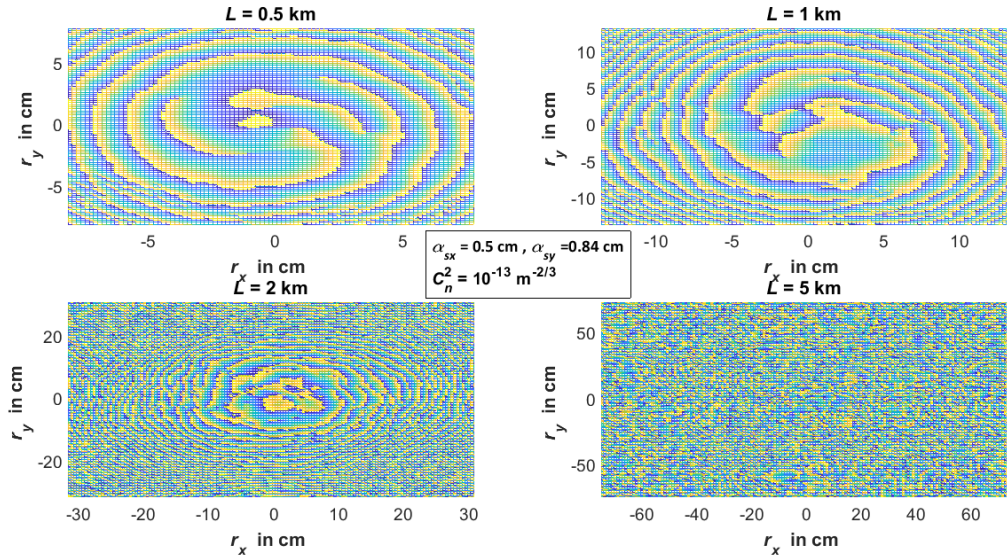**Figure 19** Phase distribution of bottle beam with source settings $\alpha_{sx} = 0.5$ cm and $\alpha_{sy} = 0.84$ cm when $C_n^2 = 10^{-13}\,\mathrm{m}^{-2/3}$.
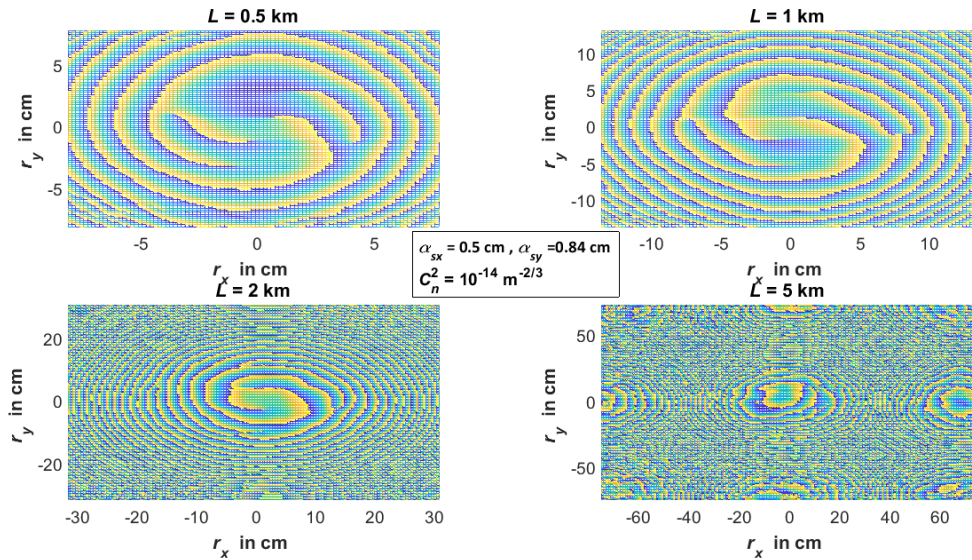
Figure 20 Phase distribution of bottle beam with source settings $\alpha_{sx} = 0.5$ cm and $\alpha_{sy} = 0.84$ cm when $C_n^2 = 10^{-14}\,\mathrm{m}^{-2/3}$.

CHAPTER 5

SCINTILLATION AND BIT ERROR RATE ANALYSIS OF BOTTLE BEAM

This part of thesis includes point like, aperture averaged scintillation for radius of receiver aperture $r = 46.9$ cm , and radius of receiver aperture $r = 105.6$ cm scintillations of selected bottle beams and the comparison between Gaussian beam. Results of point like scintillation is compared with spherical wave to see the accuracy of our simulations. All scintillation results are plotted using curve fitting function in MATLAB.

5.1 Point like Scintillation of Selected Beams

Figure 21 Point like scintillation of selected bottle beams and Gaussian beam when

$$C_n^2 = 10^{-12}\,\mathrm{m}^{-2/3}\ \ .$$

Fig. 21 illustrates the point like scintillation of selected symmetric and asymmetric large and small source size beams and comparison between Gaussian beam. As it is

seen from the figure, symmetric small source size beam has the worst scintillation performance among the selected bottle beam types and it is still better than spherical wave Gaussian beam couple. On the other hand, bottle beam with $\alpha_{sx} = 0.5$ cm and $\alpha_{sy} = 0.84$ cm is better than symmetric small source size beam with slight difference. Furthermore, both large source size bottle beams are close to each other and they are better than Gaussian beam. As it is stated in [54-55], asymmetric beams have less scintillation index than its symmetric forms.

Figure 22 Point like scintillation of selected bottle beams and Gaussian beam when $C_n^2 = 10^{-13} \text{m}^{-2/3}$.

As compared to previous Fig. 21, Fig. 22 show point like scintillation of selected bottle beams and Gaussian beam when $C_n^2 = 10^{-13} \text{m}^{-2/3}$. Similar to Fig. 21, symmetric small source size beam with settings $\alpha_{sx} = 1$ cm and $\alpha_{sy} = 1$ cm is the worst among other beams. Asymmetric large source size bottle beam with $\alpha_{sx} = 1.84$ cm and $\alpha_{sy} = 1.2$ cm is the best beam setting. Symmetric large source size bottle beam with $\alpha_{sx} = 2$ cm and $\alpha_{sy} = 2$ cm is still better than Gaussian beam and asymmetric small source size bottle beam but has higher scintillation index than asymmetric large source size bottle beam. Comparing with Fig. 21, asymmetric small source size bottle beam with $\alpha_{sx} = 0.5$ cm and $\alpha_{sy} = 0.84$ cm is still better than Gaussian beam increase in the advantage of this beam attracts the attention. For Fig.

23, weak turbulent region is valid up to 1.5 km distance and scintillation index of all beams has rising behaviour there. Furthermore, beams show decaying trend in moderate turbulence region.
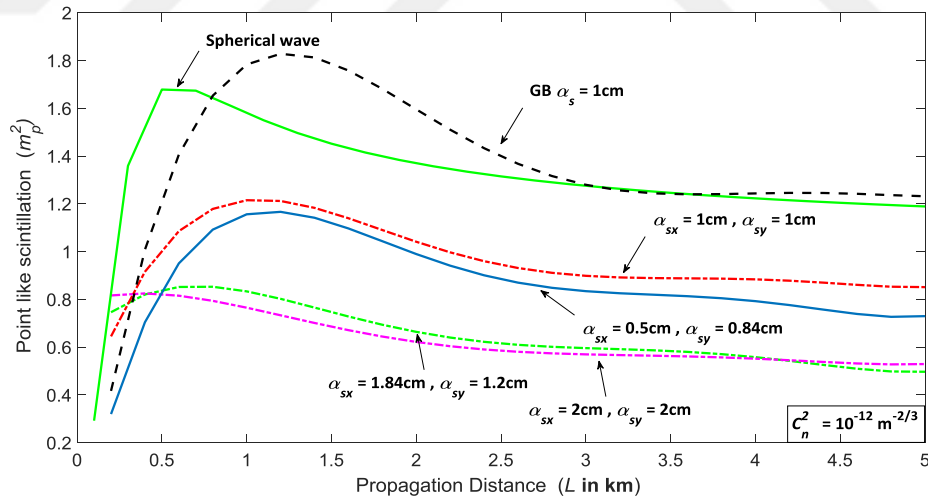

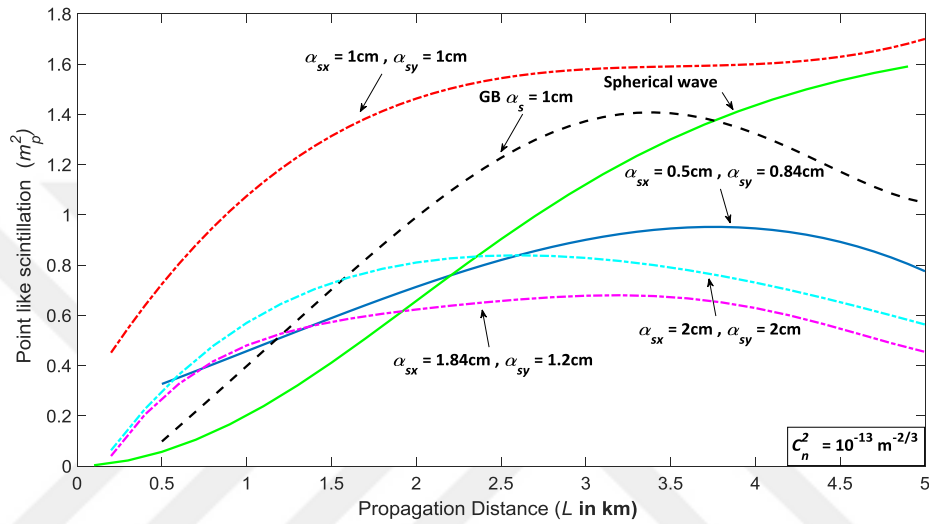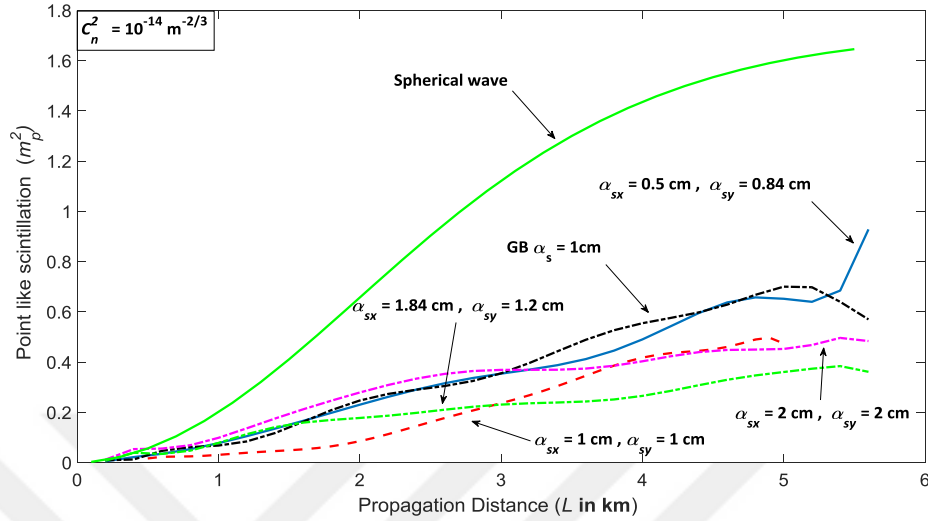**Figure 23** Point like scintillation of selected bottle beams and Gaussian beam when

$$C_n^2 = 10^{-14} \, \text{m}^{-2/3} \quad .$$

Fig. 23 shows point like scintillation comparison of selected bottle beam settings and Gaussian beam. As it is compared with Fig. 21 and Fig. 23, scintillation index of asymmetric small source size bottle beam with $\alpha_{sx} = 0.5 \, \text{cm}$ and $\alpha_{sy} = 0.84 \, \text{cm}$ increases and becomes nearly close to Gaussian beam. Other bottle beam settings symmetric small source size beam with $\alpha_{sx} = 1 \, \text{cm}$ and $\alpha_{sy} = 1 \, \text{cm}$, symmetric large source size beam with $\alpha_{sx} = 2 \, \text{cm}$ and $\alpha_{sy} = 2 \, \text{cm}$ seem advantageous for long propagation distances. Among all beams asymmetric large source size bottle beam $\alpha_{sx} = 1.84 \, \text{cm}$ and $\alpha_{sy} = 1.2 \, \text{cm}$ is the best for weak turbulence settings. Furthermore, scintillation index of all beams decreases while turbulence decreases as it is seen from Fig. 21 and Fig. 22 above. In comparison amon Fig. 21, Fig. 22, and Fig. 23 above, scintillation index shows raising behavior in weak turbulent region in all. All beams show rising behaviour in weak turbulent region, have decaying profile in moderate turbulent region, and have saturated trend for strong turbulence regions as it is stated in [27].

5.2 Aperture Averaged Scintillation of Selected Beams for Small Aperture

Figure 24 Aperture averaged scintillation of selected bottle beams and Gaussian beam when $C_n^2 = 10^{-12}\,\mathrm{m}^{-2/3}$ and $r_{x1,y1} = 42\ cm$.

Fig. 24 illustrates aperture averaged scintillation of selected bottle beams and Gaussian beam for structure constant $C_n^2 = 10^{-12}\,\mathrm{m}^{-2/3}$. In case of aperture averaged scintillation, symmetric large source size beam has the least scintillation index for strong turbulent region even though both symmetric and asymmetric large source size bottle beams have less scintillation index as compared to Gaussian beam. On the other hand, both symmetric and asymmetric small source size bottle beams are worse than Gaussian beam. Symmetric small source size bottle beam seems advantageous only for closer distances.

Fig. 25 shows aperture averaged scintillation for $C_n^2 = 10^{-13}\,\mathrm{m}^{-2/3}$. As opposed to point like scintillation, ratio difference between scintillation index of Gaussian beam and asymmetric small source size bottle beam increases while structure constant decreases. Additionally, this type of beam becomes advantageous while turbulence decreases. As it is in general, either both large source size beam are advantageous or difference advantage with respect to Gaussian beam increases sharply. Although symmetric small source size bottle beam is disadvantageous, thip type of beam takes

the advantage for closer distances up to 1 km. Since there is so much difference among these beams, plot is shown as logaritmic scale. Comparing with Fig. 24 and Fig. 25, scintillation index of all beam types decreases since turbulent level decreases.

Fig. 26 includes aperture averaged scintillation of all selected beam types when $C_n^2 = 10^{-14} \text{m}^{-2/3}$. As opposesed to other investigations, all type of beams have decaying profile up to some distance, then they reach the lowest peak value and show raising trend. Similar with the previous results, symmetric small source size bottlem beam where $\alpha_{sx} = 1 \text{ cm}$ and $\alpha_{sy} = 1 \text{ cm}$ has the highest scintillation index for longer distances although it takes the advantage for closer distances. Both symmetric and asymmetric large source size bottle beam have sharp decaying behaviour up to 1 km and then they show increasing trend. Asymmetric small bottle beam is still advantageous and located somewhere between Gaussian and large source size bottle beams.
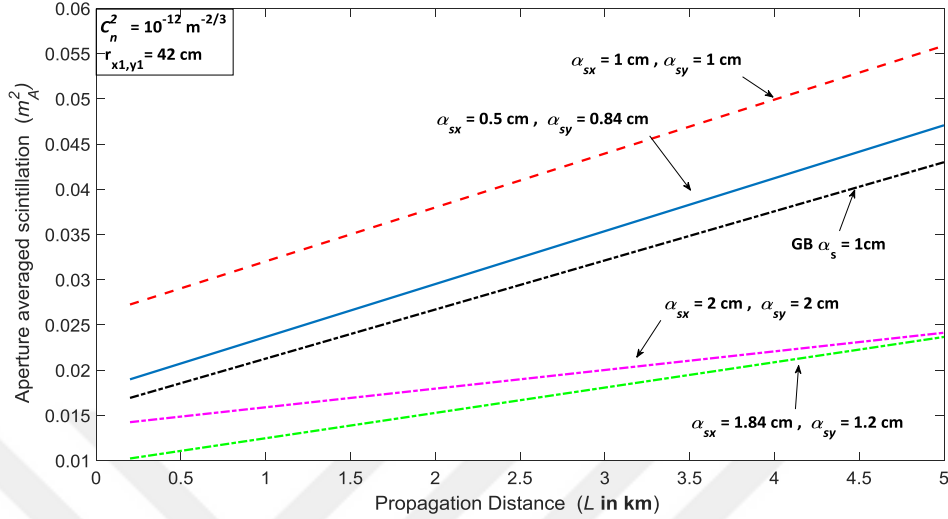

Figure 25 Aperture averaged scintillation of selected bottle beams and Gaussian beam when $C_n^2 = 10^{-13} \text{m}^{-2/3}$ and $r_{x1,y1} = 42 \, cm$.

Figure 26 Aperture averaged scintillation of selected bottle beams and Gaussian beam when $C_n^2 = 10^{-14}\,\text{m}^{-2/3}$ and $r_{x1,y1} = 42\ cm$.

5.3 Aperture Averaged Scintillation of Selected Beams for Large Aperture

Figure 27 Aperture averaged scintillation of selected bottle beams and Gaussian beam when $C_n^2 = 10^{-12}\,\text{m}^{-2/3}$ and $r_{x1,y1} = 95\ cm$.

Fig. 27 indicates aperture averaged scintillation of all selected beams when $C_n^2 = 10^{-12}\,\text{m}^{-2/3}$. Comparing with vertical axis values of Fig. 23 and Fig. 27, scintillation index of all selected beams reduces while receiver aperture increases as

48

Fried states in [45]. Symmetric large source size beam where $\alpha_{sx} = 2$ cm and $\alpha_{sy} = 2$ cm has still the least scintillation index and asymmetric form where $\alpha_{sx} = 1.84$ cm and $\alpha_{sy} = 1.2$ cm follows it. Main difference between Fig. 23 and Fig. 27 is positions of small source size beams. This time symmetric small source size bottle beam with $\alpha_{sx} = 1$ cm and $\alpha_{sy} = 1$ cm takes the advantage if larger receiver aperture is used. However asymmetric small source size beam where $\alpha_{sx} = 0.5$ cm and $\alpha_{sy} = 0.84$ cm seems disadvantageous for long distances, it becomes advantageous for longer distances and it is the least scintillation index for closer distances. All beams in Fig. 27 have raising trend in weak fluctuation regon, stable behavior in moderate fluctuaton region, and decaying profile in strong fluctuation region.
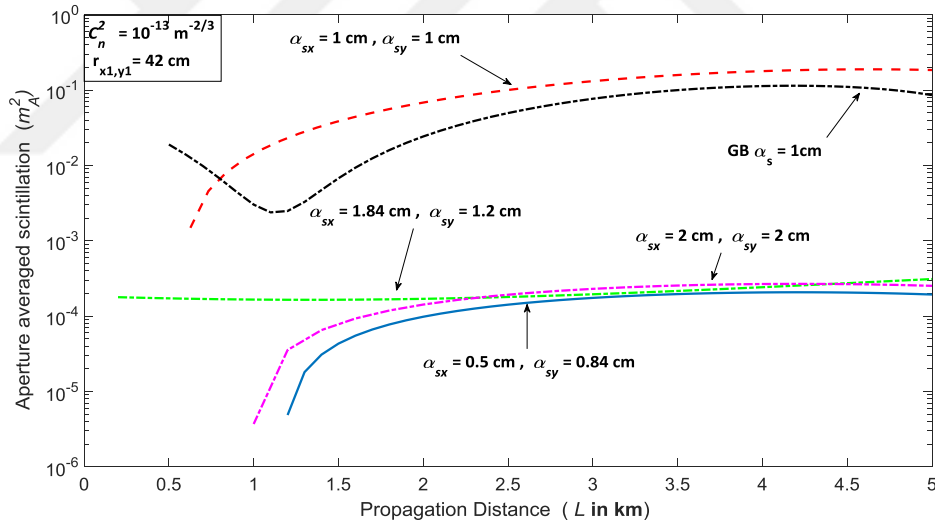

Figure 28 Aperture averaged scintillation of selected bottle beams and Gaussian beam when $C_n^2 = 10^{-13} \, \text{m}^{-2/3}$ and $r_{x1,y1} = 95 \, cm$.
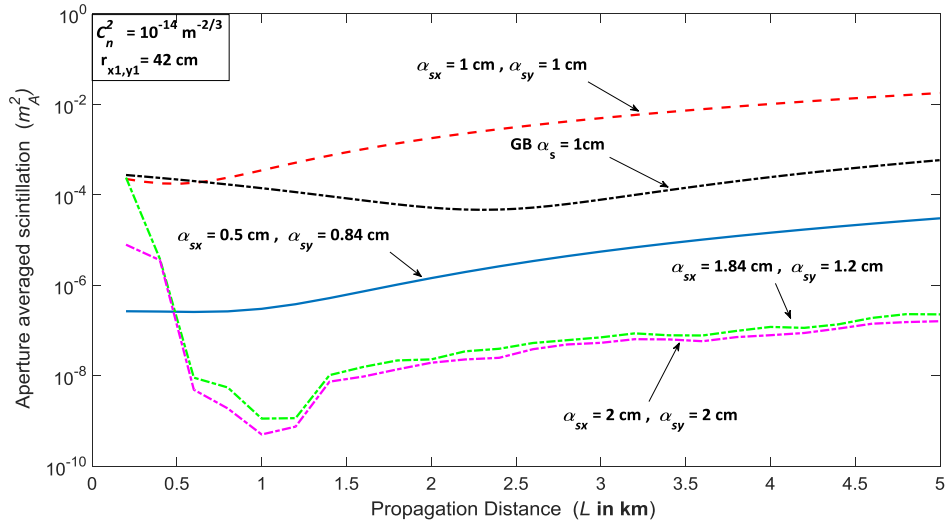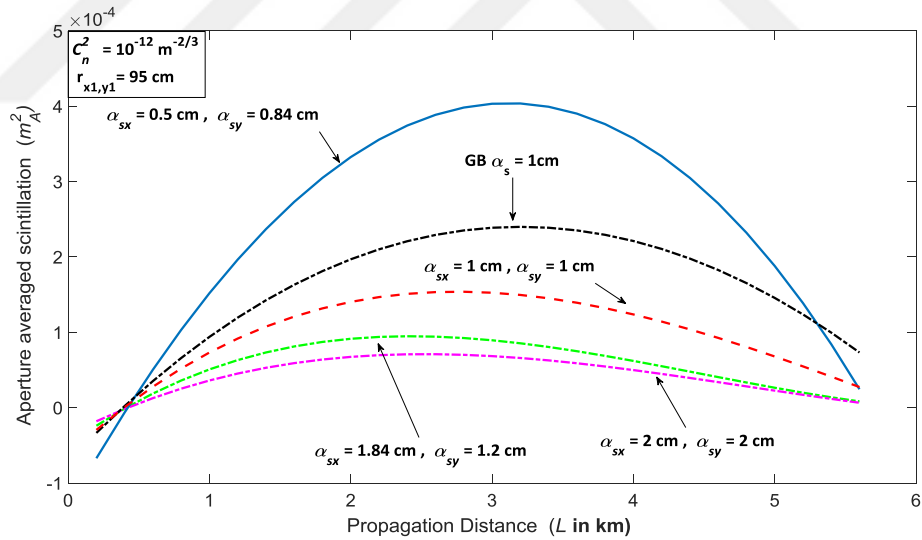
Fig. 28 shows aperture averaged scintillation of selected beams when $C_n^2 = 10^{-13} \, \text{m}^{-2/3}$. As compared to stronger turbenlence with the same aperture opening in Fig. 26, rational difference between scintillation indexes of selected beams increases. Symmetric large source size beam with $\alpha_{sx} = 2$ cm and $\alpha_{sy} = 2$ cm has the best scintillation index and asymmetric large beam with $\alpha_{sx} = 1.84$ cm and $\alpha_{sy} = 1.2$ cm follows it. Altough, symmetric small source size

beam is advantageous for long distances, both small source size beams have higher scintillation index than Gaussian beam. As compared to Fig. 25 scintillation index of all beam diminishes. Moreover, asymmetric small source size beam where $\alpha_{\text{sx}} = 0.5$ cm and $\alpha_{\text{sy}} = 0.84$ cm loses its advantage against Gaussian beam while receiver aperture increases. Asymmetric large source size beam has still less scintillation index however difference between Gaussian beam is lowered.

Fig. 29 investigates aperture averaged scintillation of selected beams for $C_n^2 = 10^{-14} \text{m}^{-2/3}$. For weak turbulent region, both small source size beams show approximately the same performance with Gaussian beam but asymmetric small source size beam has little advantage against Gaussian beam. As it is in general, symmetric large source size beam where $\alpha_{\text{sx}} = 2$ cm and $\alpha_{\text{sy}} = 2$ cm shows the best peformance while both large source size beams have less scintillation index. Comparing with Fig. 26, scintillation indexes of small source size beams comes closer with Gaussian beam. Rational difference between both large source size beams with Gaussian beam also decreases.
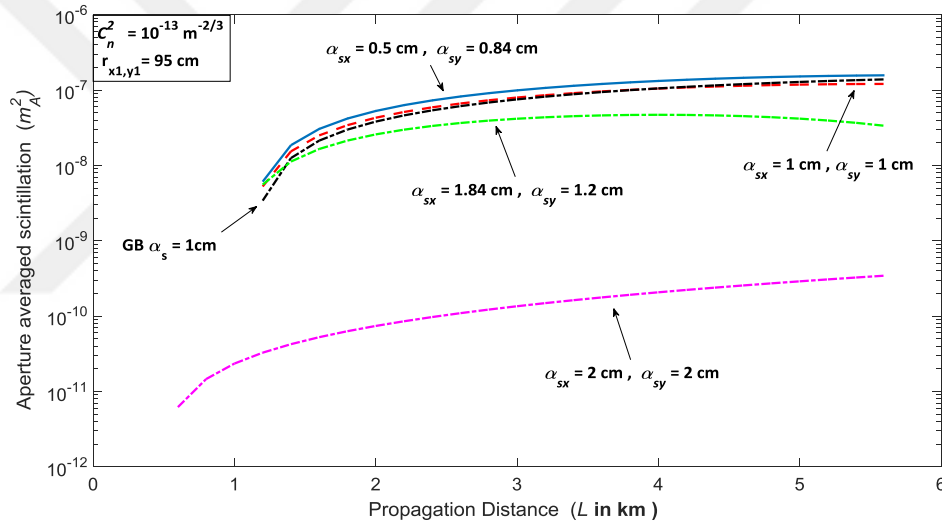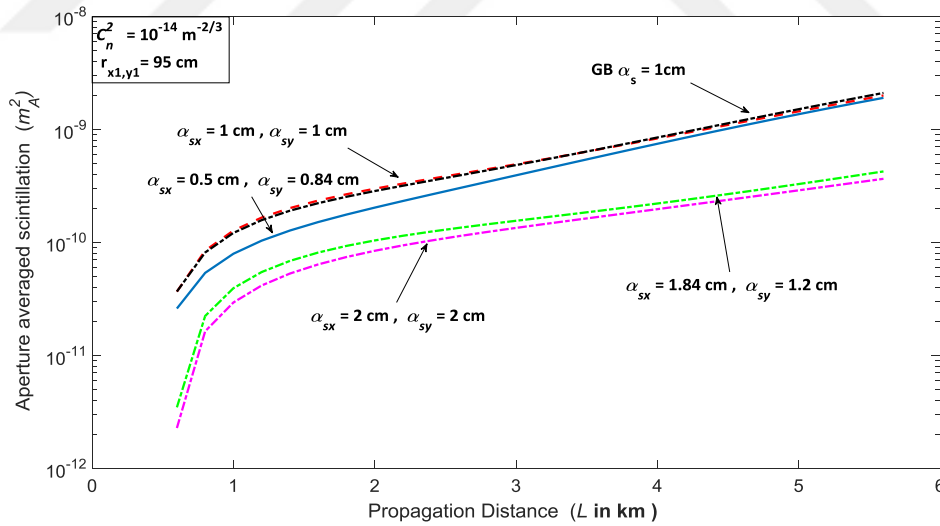

Figure 29 Aperture averaged scintillation of selected bottle beams and Gaussian beam when $C_n^2 = 10^{-14} \text{m}^{-2/3}$ and $r_{x1,y1} = 95\ cm$.

5.4 Received Power and Signal to Noise Ratio Analysis

Fig. 30 indicates received power analysis of selected beams versus structure constant at 3.3 km link distance using point like aperture. In this part of the thesis source power of all selected beams are set as 21mW to make a meaningful comparison. As it is seen from Fig. 30, more power is captured at the receiver if both small source size bottle beams are used in weak turbulent region. Moving through the turbulent region symmetric large souce size bottle beam seems advantageous with a small difference comparing with Gaussian beam.
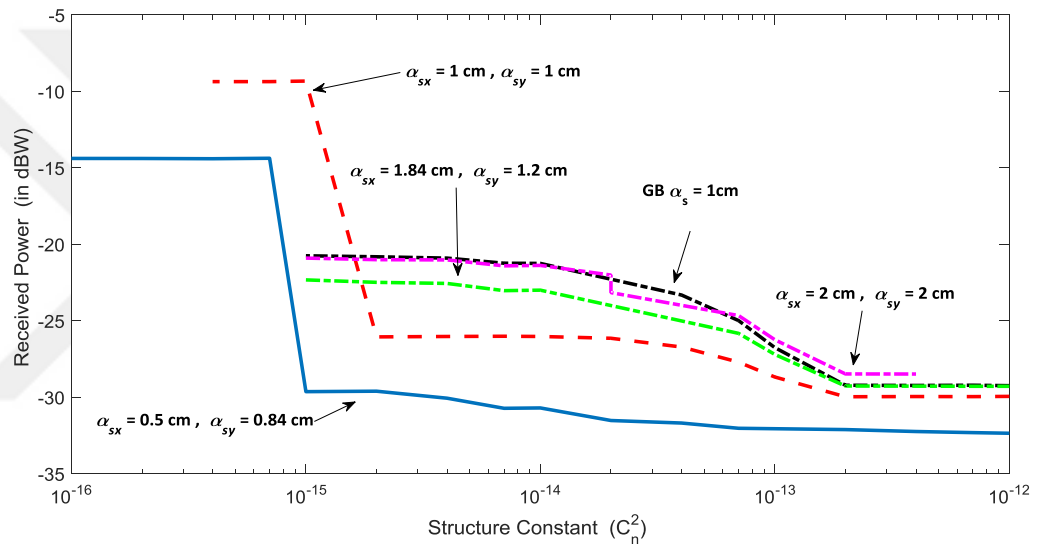
Figure 30 Received power comparison of selected beams with respect to structure constant

Fig. 31 shows the signal to noise ratio analysis of selected beams against sturcture constant. Results of this figure are similar with Fig. 30 above. While symmetric bottle beam is the most advantageous and asymmetric form follows it under weak turbulent region. Symmetric large source size bottle beam again take the lead under strong turbulence comparing with Gaussian beam and asymmetric large source size beam.

51
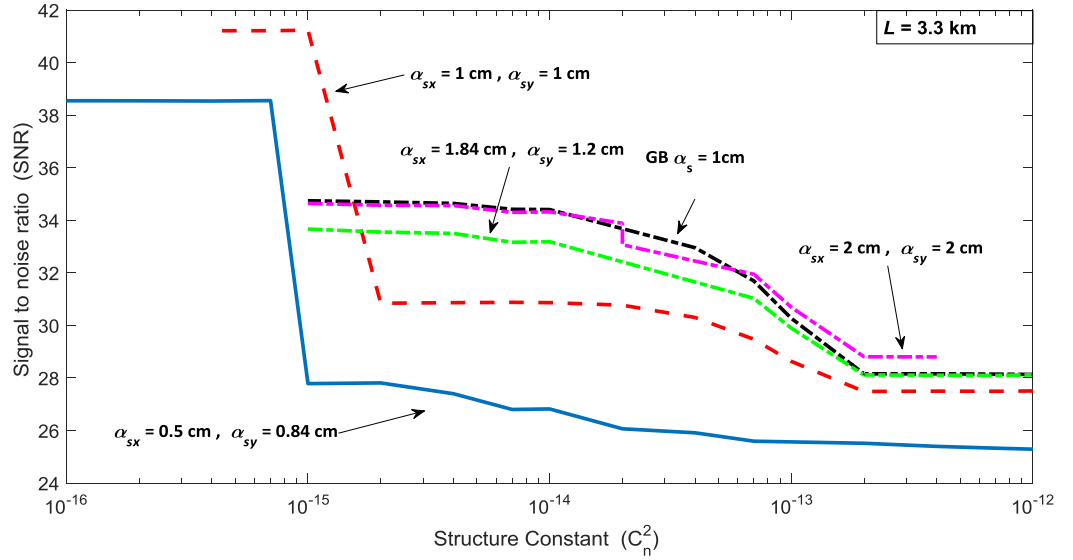
Figure 31 Signal to noise ratio comparison of selected beams with respect to structure constant

5.5 Bit Error Rate Estimation

In this part of the thesis bit error rate estimation of selected bottle beams is done and results are compared with the analytical formula. Dashed lines belong to experimental results and solid lines regard to analytical results in Fig. 32 and Fig. 33. Fig. 32 shows the bit error rate behaviors of selected beams versus structure constant. Except asymmetric small source size bottle beam under weak turbulent region, all bottle beam settings are advantageous as compared to Gaussian beam. Asymmetric large source size bottle beam has the least bit error rate value for all conditions since its scintillation index is the least one. Even though symmetric large source size bottle beam is worse than corresponding asymmetric one, it is still better than Gaussian beam in terms of bit error rate. Asymmetric small souce size beam becomes advantageous comparing with corresponding symmetric one from moderate to strong turbulence. All analytical and experimental results show the similar behaviour with a slight difference.
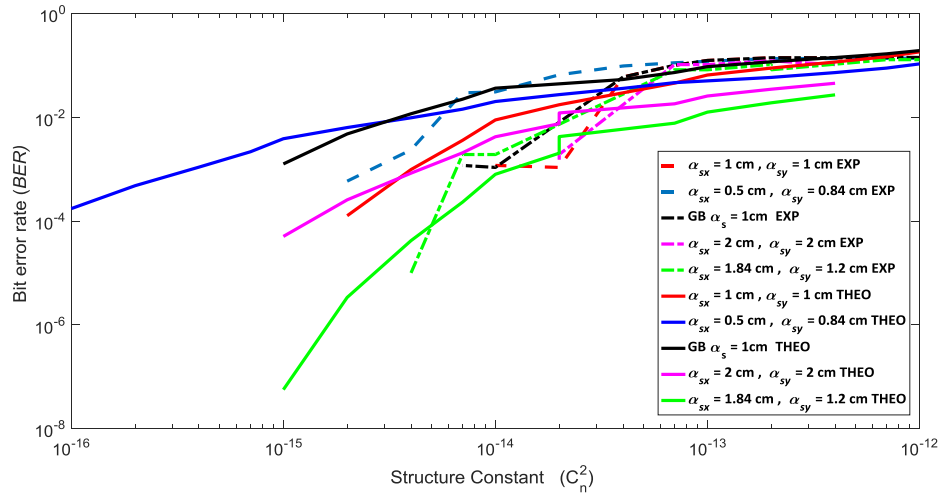
Figure 32 Bit error rate comparison of selected beams with respect to structure constant
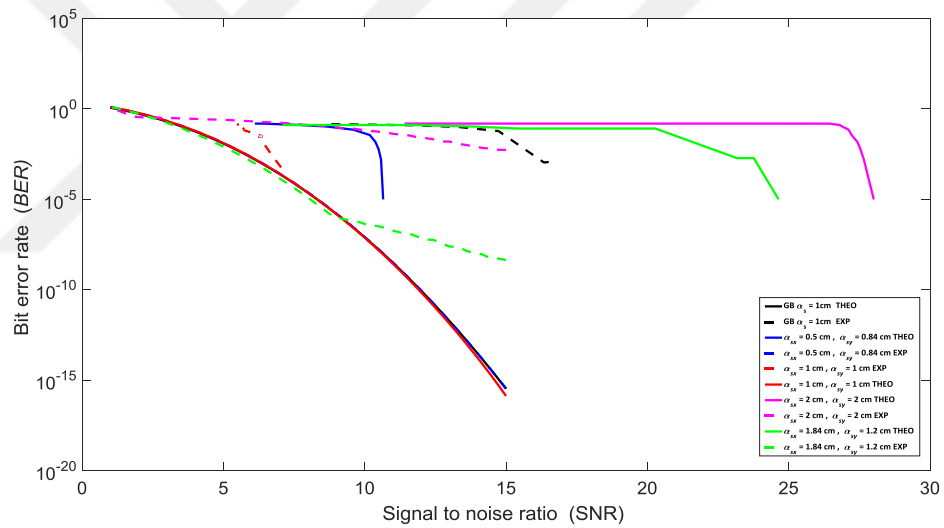
Figure 33 Bit error rate comparison of selected beams with signal to noise ratio

Fig. 33 investigates bit error rate of all selected beams versus signal to noise ratio. All bottle beam settings seem advantageous under SNR is 30dB. Similar with Fig. 32, asymmetric large source size bottle beam takes the lead in bit error rate analysis versus SNR. Corresponding symmetric one follow it. Asymmetric small source size bottle beam has less bit error rate value up to 34dB SNR then it becomes advantageous against Gaussian beam. Additionally, symmetric small source size bottle beam loses its advantage after 30dB SNR. All experimental results are suitable

with analytical results except bit error rate of asymmetrical small source size bottle beam decreases rapidly while it has slowly decreasing behavior in theoretical point of view.

CHAPTER 6

SCINTILLATION AND BIT ERROR RATE ANALYSIS OF SINE HOLLOW BEAM

This part of thesis includes point like, aperture averaged scintillation, and bit error rate analysis of sine hollow beam adapting from [94].

6.1 Point like Scintillation of Selected Beams

Figure 34 Point like scintillation of selected sine hollow beams and Gaussian beam when $C_n^2 = 10^{-12} \mathrm{m}^{-2/3}$.

Fig. 34 shows point like scintillation of sine hollow beam under strong turbulent regime. However, we operate in strong turbulence, second order normal beam and anomalous beam with $a=1, b=2, n=1$ have lower scintillation index than Gaussian beam and spherical wave couple. In addition, first order normal sine hollow beam brings a small advantage. Lastly, other anomalous beam with $a=2, b=1, n=1$ seems

advantageous in closer distances than 2.5km, although it loses its advantage after that distance. All types of beams show rising trend in weak turbulent region, decaying behaviour in moderate turbulent region, and saturated behavior in strong turbulent region.
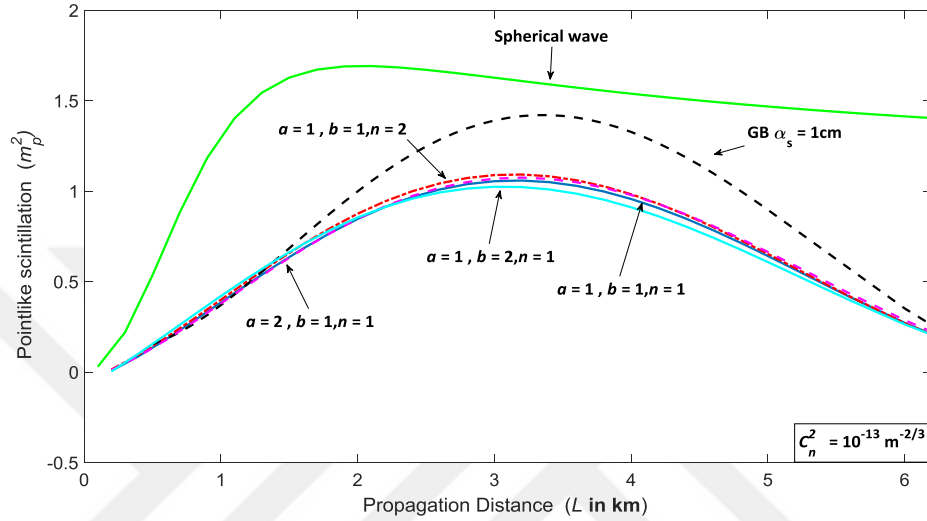
Figure 35 Point like scintillation of selected sine hollow beams and Gaussian beam when $C_n^2 = 10^{-13} \, \text{m}^{-2/3}$.

In Fig. 35, we see point like scintillation of sine hollow beam in weaker turbulence than previous figure. We investigate that all beams have less scintillation index than spherical wave. Selected sine hollow beams have less scintillation index than Gaussian beam between 1-5.6km distances. In this region, there is not a significant difference among sine hollow beam types. After 5.6km, Gaussian beam takes the advantage and all beams have saturated trend nearly $m_p^2 = 0$ since inner scale length $l_0 = 0$ converges into Kolmogorov spectrum. Fig. 36 presents point scintillation of sine hollow beam under weak turbulent conditions. Under this turbulent regime, all types of sine hollow beam have less scintillation index than Gaussian beam and spherical wave. Similar with Fig. 35, there is not a remarkable difference among sine hollow beams.
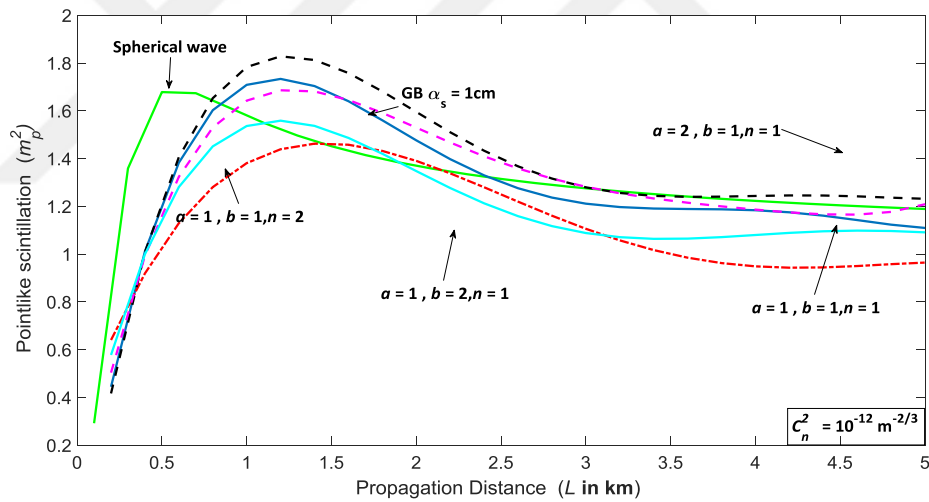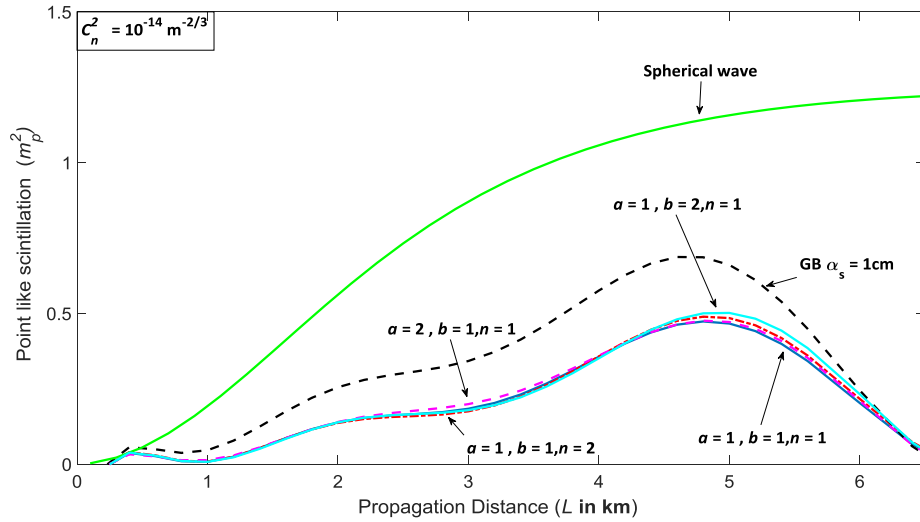
Figure 36 Point like scintillation of selected sine hollow beams and Gaussian beam when $C_n^2 = 10^{-14} \, \text{m}^{-2/3}$.

6.2 Aperture Averaged Scintillation of Selected Beams

Fig. 37 shows aperture averaged scintillation of sine hollow beam under strong turbulent regime. Radius of receiver aperture is taken as $r_r = 78 \, cm$ to make a clear comparison between bottle beam and sine hollow beam. According to this figure, all types of sine hollow beam have less scintillation index than Gaussian beam up to 3.5km distance. After that distance first order normal and anomalous sine hollow beams with $a > b$ become disadvantageous. Remaining anomalous beam has a sligth advantage in longer distance, however advantage is bigger in closer distance. Under this condition, second order normal beam has the least scintillation index in all propagation distance.
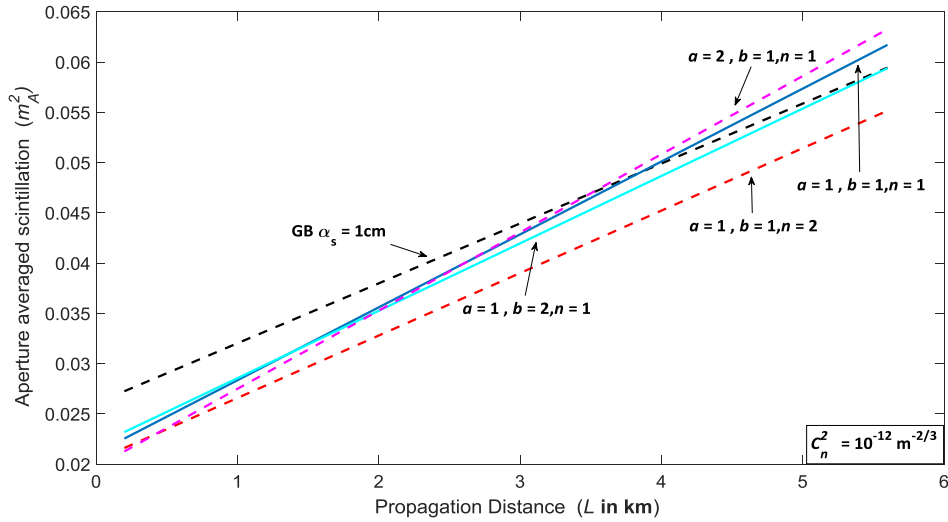
Figure 37 Aperture averaged scintillation of selected sine hollow beams and Gaussian beam when $C_n^2 = 10^{-12}\,\mathrm{m}^{-2/3}$.
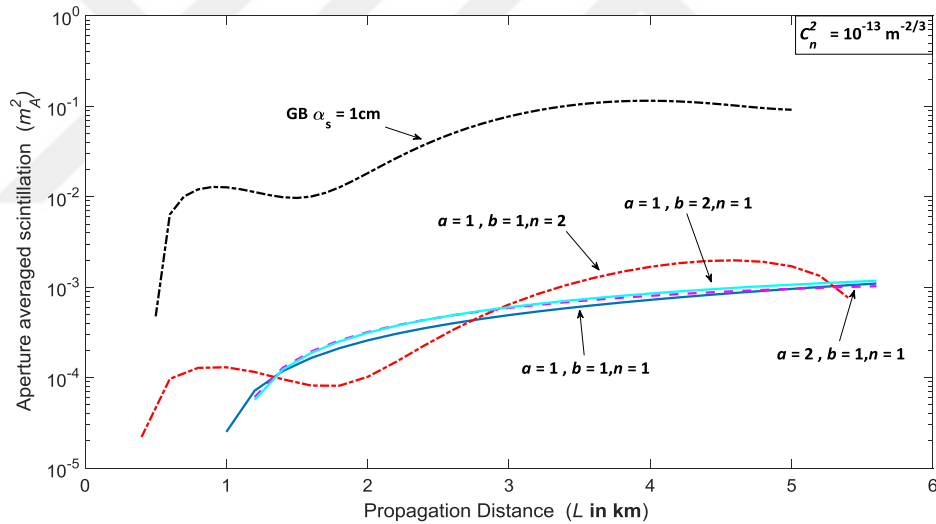
Figure 38 Aperture averaged scintillation of selected sine hollow beams and Gaussian beam when $C_n^2 = 10^{-13}\,\mathrm{m}^{-2/3}$.

Fig. 38 indicates aperture averaeged scintillation of SHB when $C_n^2 = 10^{-13}\,\mathrm{m}^{-2/3}$. As compared to Fig. 37, difference between Gaussian beam and selected sine hollow beams increases. That's why, Fig. 38 and 39 is plotted in log scale. In closer and longer distances, anomalous beams seem advantageous while second order normal sine hollow beam has less scintillation index in moderate propagation distance. Furthermore, first order normal sine hollow beam shows similar performance with

58

anomalous SHBs. Looking at Fig. 39, we investigate that all SHBs have extreamly less scintillation index than Gaussian beam under moderate turbulent condition. Second order normal SHB brings less advantage comparing with anomalaous and first order normal SHB but still better than Gaussian beam. First order normal beam and anomalous beams show similar trend with advantage of 100 times better than Gaussian beam.
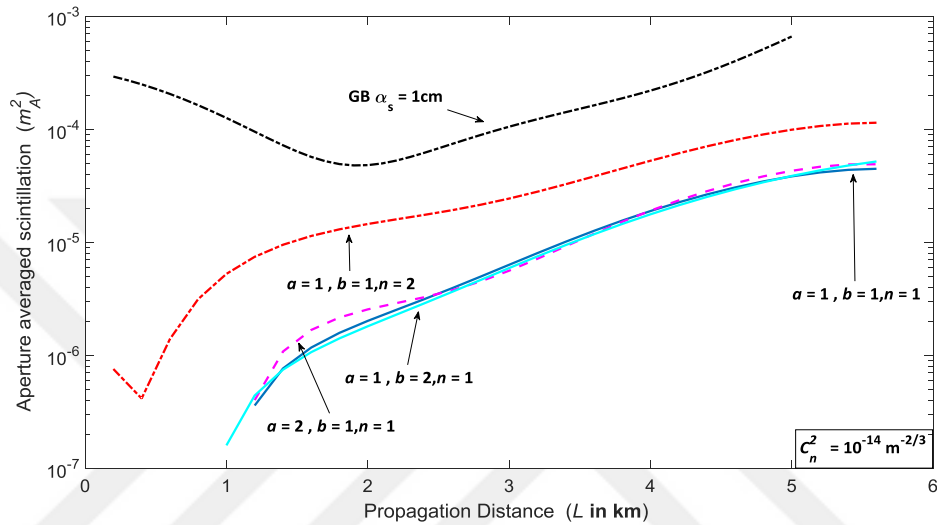
Figure 39 Aperture averaged scintillation of selected sine hollow beams and Gaussian beam when $C_n^2 = 10^{-14}\,\mathrm{m}^{-2/3}$.

6.3 Bit Error Rate Analysis of Sine Hollow Beam
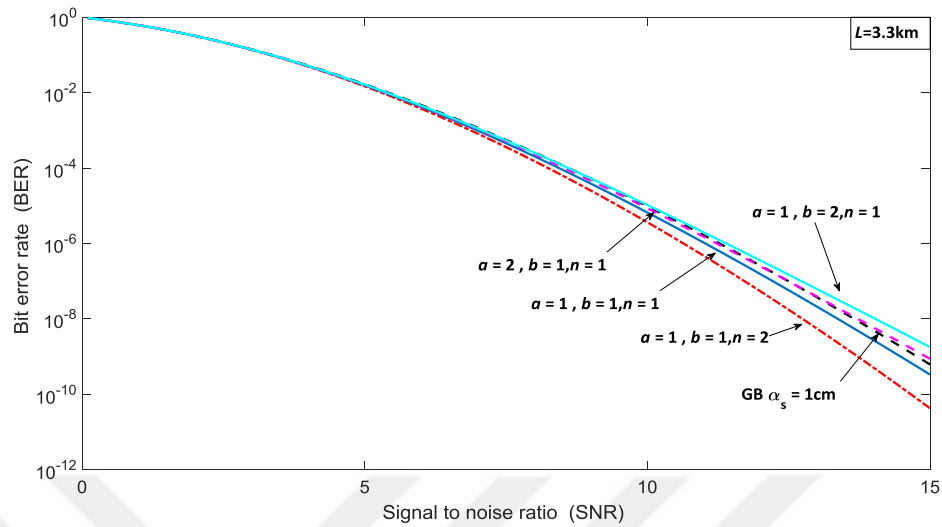
Figure 40 Bit error rate analysis of sine hollow beam against signal to noise ratio.

Fig. 40 presents bit error rate performance of SHB against SNR in 3.3.km link distance. Our results show that normal SHBs have less BER where second order beam has a sligth advantage. In case of anomalaous SHBs, this type of beams have less BER for low SNR. On the other hand, anomalaous beams have higher BER for high SNR. Fig. 41 shows BER analysis of SHBs against turbulence strength. Similar with Fig. 40, normal SHBs have less BER than Gaussian beam in all turbulent conditions while second order beam takes the lead. Anomalous beams show better performance in strong turbulent regime while they have higher BER than Gaussian beam in weaker turbulence.
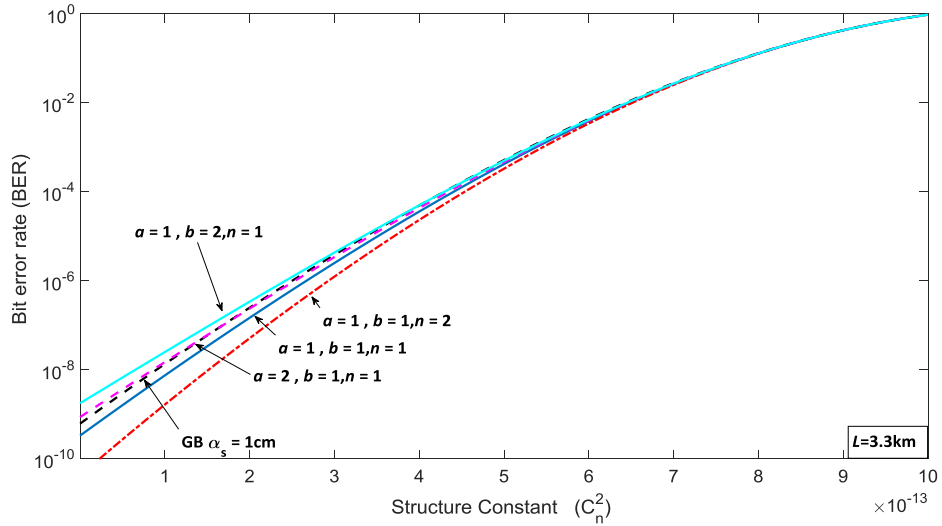
Figure 41 Bit error rate analysis of sine hollow beam against refractive index structure constant

6.4 Scintillation and BER Comparison of BB and SHB
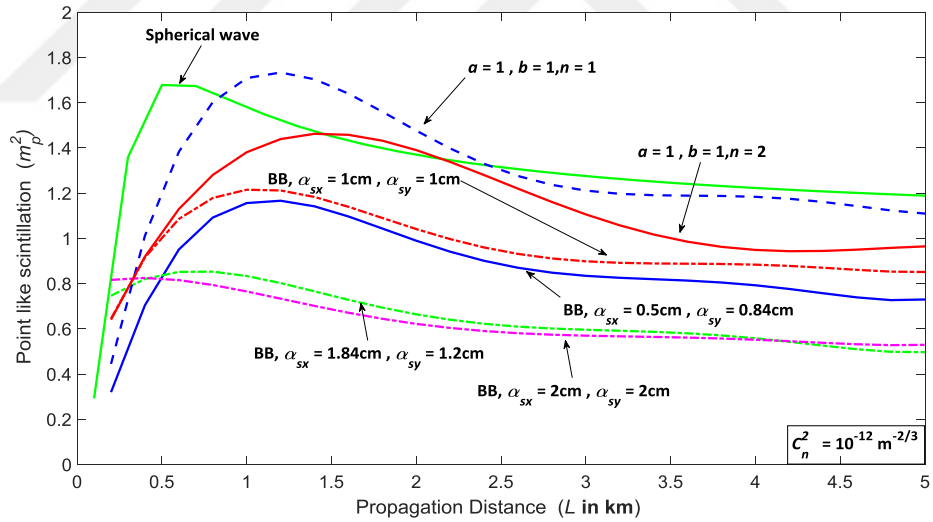
Figure 42 Point like scintillation comparison of BB and SHBs when

$$C_n^2 = 10^{-12}\,\mathrm{m}^{-2/3} \quad.$$
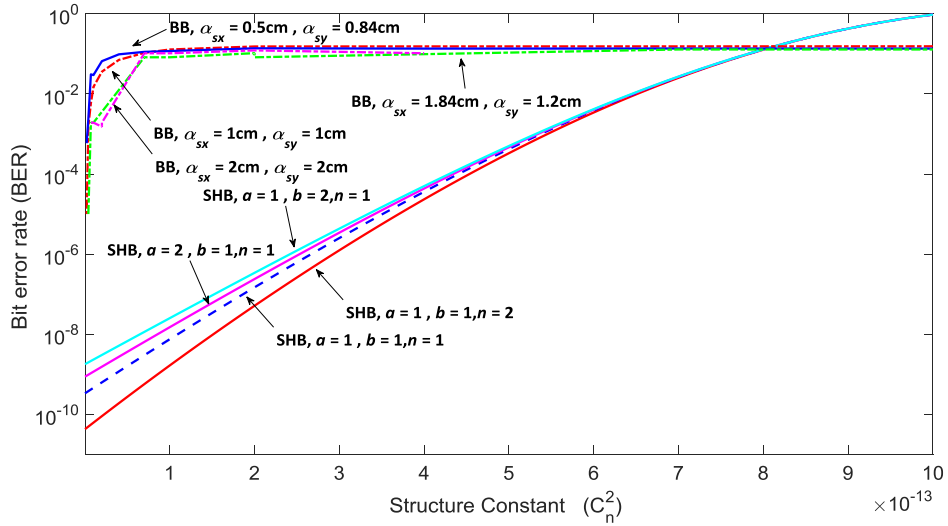
Figure 43 Bit error rate comparison of BB and SHB versus refractive index structure constant.
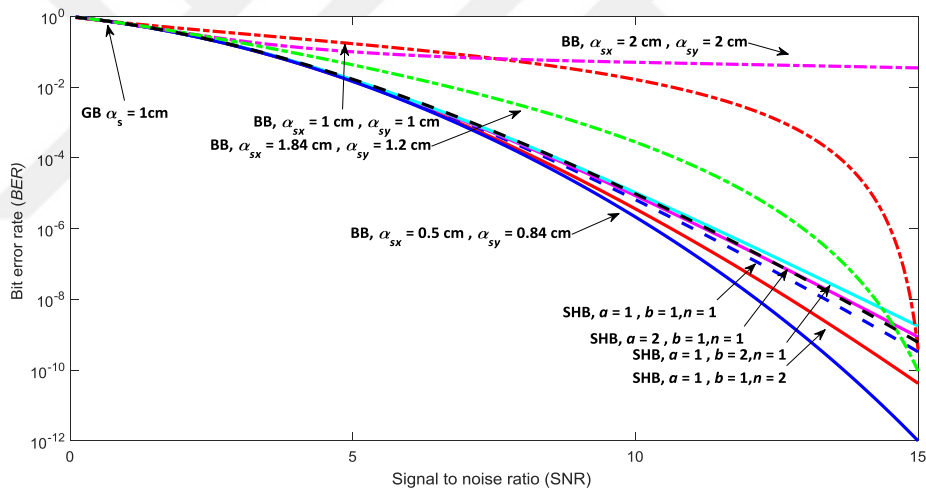
Figure 44 Bit error rate comparison of BB and SHB versus signal to noise ratio.

In this part of the thesis, we conclude our study comparing point like scintillation under strong turbulence in Fig. 42 and bit error rate of bottle beam (error counting values) and sine hollow beams in Fig. 43 and 44. Looking at Fig. 42, we investigate that scintillation index of not only large source size bottle beam but also small source size beam is lower than sine hollow beams. This brings us in Fig. 43, selected bottle beams show better performance in strong turbulent region in BER point of view. As turbulent strength decreases, sine hollow beams get the advantage. In this figure

results from error counting method using bottle beam and analytical results of sine hollow beam is compared. In addition to this, we compare all analytical bit error rate values of both bottle and sine hollow beams in Fig. 44. As an investigation of this figure, we can say that it seems possible to reduce bit error rate 10^{-3} times by increasing SNR value. This advantage can be achieved using asymmetric small source size bottle beam which has $\alpha_{sx} = 0.5$cm and $\alpha_{sy} = 0.84$cm . Furthermore, second order and first order normal sine hollow beams provides less bit error rate compared with Gaussian beam. Anomalous sine hollow beams does not change the system performance. Asymmetric large source size bottle beam having $\alpha_{sx} = 1.84$cm and $\alpha_{sy} = 1.2$cm shows an interesting trend as compared to Gaussian beam. While this type of beam is disadvantageous in low SNR, it has lowe BER value after 14 dB SNR. Similar with this type of beam, symmetric small source size bottle beam where $\alpha_{sx} = 1$cm and $\alpha_{sy} = 1$cm takes the advantage nearly after 15 dB SNR. Lastly, asymmetric large source size bottle beam has the highest bit error rate value for all covered SNR regions.

CHAPTER 7

CONCLUSION

In this study, propagation features, kurtosis parameters, scintillation expectation, and BER estimation of bottle beams are studied. analytical expression of scintillation is derived up to last step via Rytov method. Analytical derivation gives the idea of asymmetrical bottle beams have less scintillation value because solution involves coupling terms of Gaussian source sizes. Since integral becomes too complicated to solve, we turn into numerical simulation method which is random phase screen. Benefiting from random phase screen approach, phase distribution of vortex added bottle beam, intensity profiles, point like and aperture averaged scintillation index, SNR, and BER values are obtained. Four different bottle beam settings are selected as small and large source sizes and asymmetric forms with equal power to the corresponding source sizes. Bottle beam is suitable for orbital angular momentum applications. Although, there is phase term in the bottle beam expression, we add $\exp(-jn\phi)$ term to carry the information via topological charge. Results show that FSO links which carry information using topological charge can be established up to 1km link distance in strong turbulence. Looking at intensity profiles, we investigate that asymmetric bottle beams protects their shapes more than their symmetric forms along propagation axis. In the comparison of small and large source size bottle beams, large source size beams especially asymmetric one are affected less than small source size beams. These investigations will provide an insight large source size beams have less scintillation index. Moreover, asymmetric bottle beams have also less scintillation index as compared to their congruent symmetric forms. In another point of view, effect of aperture size and turbulence strength is analyzed in detail. Scintillation index of all beams increases while structure constant increases. Additionally, property of scintillation index and receiver aperture size is inversely

proportional to each other is verified one more time in this study. In all scintillation runs, source power of all beams are set as unity to make a clear comparison and compared with the Gaussian beam having unit source size and spherical wave formulated in literature. Results show that large source size bottle beams are advantageous for cases of scintillation. Asymmetric small source size bottle beam goes up first in the comparison among small source size beams and Gaussian beam. During the communication test, link distance is fixed to 3.3km 100000 bits are transmitted. Source powers of all beams are set as 21mW. In the analysis of received power and SNR, we show that small source size beams have higher values in weak and moderate turbulent region. On the other hand, symmetric large source size bottle beam takes the advantage in strong turbulent region. Bit error rate analysis of this thesis is done via numerical simulation and analytical verification. This analysis brings us usage of bottle beam with all settings decreases the bit error rate value considering from the weak turbulent region to strong turbulent region. Furthermore, usage of bottle beam reduces probability of error comparing with Gaussian beam although SNR is low.

In the comparison of BB and SHBs, we see that bottle beams are more resistive to atmospheric turbulence. In other words, point like scintillation index of bottle beams is sufficiently lower than best of sine hollow beams. This advantage reflects into BER performance of these beams. Bottle beams show better performance in BER point of view as compared to sine hollow beams under strong turbulent conditions. However, SHBs catch the advantage for weak turbulent regimes. Our results show that usage of asymmetric small source size bottle beam reduces bit error rate 10^{-3} times lower than Gaussian beam. Besides this, it is possible to obtain less BER than Gaussian beam if second order and first order normal sine hollow beams. If system opeartes more than 14 dB SNR at the receiver, symmetric small and asymmetric large source size bottle beams can be added to preference list.

In conclusion, usage of bottle beam for optical wireless communication links under turbulent atmosphere increases the system performance reducing the bit error rate. Since it has less intensity fluctuation as compared to Gaussian beam. If the system operates in weak turbulent region, we suggest usage of sine hollow beams. Since its BER is lower than bottle beams for these conditions. We believe that this

study open a new window for FSO and LIDAR system designers. New designed OWC systems with bottle beam and sine hollow beam can be used in 5G/6G because of its low BER performance.

REFERENCES

1. **Arlt J. and Padget M. J., (2000),** "*Generation of a beam with a dark focus surrounded by regions of higher intensity: the optical bottle beam*", Opt. Lett., vol. 25, pp. 191-193.

2. **Du T., Wang T., Wu F., (2014),** "*Generation of three-dimensional optical bottle beams via focused non-diffracting Bessel beam using an axicon*", Opt. Commun., vol. 317, pp 24-28.

3. **Raman S., Yadav B. K., Bisht N. S., Husain M., Kandpal H. C., (2009),** "*A simple experimental method to generate partially coherent optical bottle beam*", Opt. Laser. Eng., vol. 47, pp. 1282-1285.

4. **Wei M., Shiao W., Lin Y., (2005),** "*Adjustable generation of bottle and hollow beams using axicon*", Opt. Commun., vol. 248, pp. 7-14.

5. **Philip G. M. and Viswanathan K., (2010),** "*Generation of tunable chain of three-dimensional optical bottle beams via focused multi-ring hollow Gaussian beam*", J. Opt. Soc. Am. A, vol. 27, pp. 2394-2401.

6. **Rao L., Zheng X., Wang Z., Yei P., (2008),** "*Generation of optical bottle beams through focusing J0-correlated Schell-model vortex beams*", Opt. Commun., vol. 281, pp. 1358-1365.

7. **Wei M., (2007),** "*Generation of bottle beam by focusing a super-Gaussian beam using a lens and an axicon*", Opt. Commun., vol. 277, pp. 19-23.

8. **McGloin D., Spalding G. C., Melville H., Sibbet W., Dholakia K., (2003),** "*Three-dimensional arrays of optical bottle beams*", Opt. Commun., vol. 225, pp. 215-222.

9. **Ye H., Wan C., Huang K., Han T., Teng J., Ping Y. S., Qiu C., (2014),** "*Creation of vectorial bottle-hollow beam using radially or azimuthally polarized light*", Opt. Lett., vol. 39, pp. 630-633.

10. **Lin J., Liang H., Hsieh W., (2007),** "*Generation of Supercontinuum Bottle beam using an axicon*", Opt. Express, vol. 15, pp. 2940-2946.

11. **Chen Y., Yan L., Steinvurzel P., Ramachardan S., (2012),** "*Bottle beam generation from fiber-based Bessel beams*", Conference on Lasers and EO, ISSN 2160-8989.

12. **Szulzycki K., Savarin V., Grulkowski I., (2016),** "*Generation of dynamic Bessel beams and dynamic bottle beams using acousto-optic effect*", Opt. Express, vol. 24, pp. 23977-23991.

13. **Ahluwalia B. P. S., Yuan X-C., Tao S. H., (2004),** "*Generation of self-imaged optical bottle beams*", Opt. Commun., vol. 238, pp. 177-184.

14. **Li L., Lee W. M., Xie X., Krokilikowski W., Rode A. V., Zhou J., (2014),** "*Shaping self-imaging bottle beams with modified quasi-Bessel beams*", Opt. Let., vol. 39, pp. 2278-2281.

15. **Shvedov V. G., Izdebskaya Y. V., Rode A. V., Desyatnikov A., Krokilikowski W., Kivshar Y. S., (2008),** "*Generation of optical bottle beams by incoherent white light vortices*", Opt. Express, vol. 16, pp. 20902-20907.

16. **Porfirev A. P. and Skidanov R. V., (2013),** "*Generation of an array of optical bottle beams using a superposition of Bessel beams*", App. Opt., vol. 52, pp. 6230-6238.

17. **Pu J., Liu X., Nemoto S., (2005),** "*Partially coherent bottle beams*", Opt. Commun., vol. 252, pp. 7-11.

18. **Rao L. and Pu J., (2007),** "*Generation of partially coherent vortex bottle beams*", Chin. Opt. Lett., vol. 5, pp. 379-382.

19. **Penciu R-S., Qiu Y., Goutsoulas M., Sun X., Hu Y., Xu J., Chen Z., Efreminidis N. K., (2018),** "*Observation of microscale nonparaxial optical bottle beams*", Opt. Lett., vol. 43, pp. 3878-3881.

20. **Genevet P., Dellinger J., Blanchard R., She A., Petit M., Cluzel B., Kats M. A., Fornel F., Capasso F., (2013),** "*Generation of two-dimensional plasmonic bottle beams*", Opt. Express, vol. 21, pp. 10295-10300.

21. **Epstein I. and Arie A., (2014),** "*Dynamic generation of plasmonic bottle-beams with correlated shape*", Opt. Lett., vol. 39, pp. 3165-3168.

22. **Chen C-H., Tai P-T., Hsieh W-F., (2004),** "*Bottle beam from a bare laser for single-beam trapping*", App. Opt., vol. 43, pp. 6001-6006.

23. **Xu Y., (2014),** "*Sine hollow beam and its propagation property*", Optik, vol. 125, 3465-3468.

24. **Wen W. and Chu X., (2014),** "*Propagation of symmetric tunable dual airy beam through ABCD optical system*", Opt. Commun., vol. 333, pp. 38-44.

25. **Liu H., Lü Y., Zhang J., Xia J., Pu X., Dong Y., Li S., Fu X., Zhang A., Wang C., Tan Y., Zhang X., (2015),** "*Research on propagation properties of controllable hollow flat-topped beams in turbulent atmosphere based on ABCD matrix*", Opt. Commun., vol. 334, pp. 133-140.

26. **Chafiq A., Hricha Z., Belafhal A., (2005),** "*Paraxial propagation of Mathieu beams through an apertured ABCD optical system*", Opt. Commun., vol. 253, pp. 223-230.

27. **Chafiq A., Hricha Z., Belafhal A., (2005),** "*A detailed study of Mathieu-Gaussian beams propagation through an apertured ABCD optical system*", Opt. Commun., vol. 265, pp. 594-602.

28. **Andrews L. C. and Philips R. L., (2005),** "*Laser Beam Propagation through Random Media, Second Edition*", SPIE Press, Washington.

29. **Tang H. and Ou B., (2011),** "*Beam propagation factor of radial Gaussian-Schell model beam array in non-Kolmogorov turbulence*", Opt. Laser Technol., vol. 43, pp. 1442-1447.

30. **Qin Z., Tao R., Zhou P., Xu X., Liu Z., (2014),** "*Propagation of partially coherent Bessel-Gaussian beams carrying optical vortices in non-Kolmogorov turbulence*", Opt. Laser Technol., vol. 56, pp. 182-188.

31. **Wen W., Chu X., Ma H., (2015),** "*The propagation of a combining Airy beam in turbulence*", Opt. Commun., vol. 336, pp. 326-329.

32. **Tao P., Wang X., Si L., Zhou P., Liu Z., (2013),** "*Propagation of focused vector laser beams in turbulent atmosphere*", Opt. Laser Technol., vol. 54, pp. 62-67.

33. **Schmidt J.D., (2010),** "*Numerical Simulation of Optical Wave Propagation with Examples in MATLAB*", SPIE, Washington, USA.

34. **Eyyuboğlu H. T. and Bayraktar M., (2016),** "*Propagation properties of cylindrical sinc Gaussian beam*", J. Mod. Opt., vol. 63, pp. 1706-1712.

35. **Martinez-Herrero R., Piquero G., Mejias P. M., (1995),** "*On the propagation of the kurtosis parameter of general beams*", Opt. Commun., vol. 115, pp. 225-232.

36. **Luo S, and Lü B., (2003),** "*M2 factor and kurtosis paratmeter of super-Gaussian beams passing through an axicon*", I. J. Light and El. Opt., vol. 114, pp. 193-198.

37. **Eyyuboğlu H. T., (2014),** "*Propagation analysis of Ince-Gaussian beams in turbulent atmosphere*", App. Opt., vol. 53, pp. 2290-2296.

38. **Lü B. and Wang X., (2002),** "*Kurtosis parameter of Bessel-modulated Gaussian beams propagating through ABCD optical systems*", Opt. Commun., vol. 204, pp. 91-97.

39. **Liu D. and Zhou Z., (2010),** "*Propagation and the kurtosis parameter of Gaussian flat-topped beams in uniaxial crystals orthogonal to the optical axis*", Opt. Las. Eng., vol. 48, pp. 58-63.

40. **Luo S. and Lü B., (2002),** "*Propagation of the kurtosis parameter of elegant Hermite-Gaussian and Laguerre-Gaussian beams passing through ABCD systems*", I. J. Light and El. Opt., vol. 113, pp. 227-231.

41. **Wen W., Chu X., Cai Y., (2014),** "*Dependence of the beam wander of an airy beam on its kurtosis parameter in a turbulent atmosphere*", Opt. Las. Tech., vol. 68, pp. 6-10.

42. **Zhou G.,(2009),** "The beam propagation factors and the kurtosis paramterers of a Lorentz beam", Opt. Laser Technol., vol. 41, pp. 953-955.

43. **Luo S. and Lü B., (2002),** "*Propagation of the kurtosis parameter of Hermite-cosh-Gaussian beams*", I. J. Light and El. Opt., vol. 113, pp. 329-332.

44. **Mao H., Ge F., Chen L., Shi X., (2013),** "*The influence of the bandwidth on beam propagation factor and kurtosis parameter for a broadband beam modulated by a hard-edged aperture*", Optik, vol. 124, pp. 3651-3654.

45. **Tatarski V. I., (1961),** "*Wave propagation in a turbulent medium*", McGraw-Hill, New York.

46. **Fried D. L. and Seidman J. B., (1967),** "*Laser-Beam Scintillation in the Atmosphere*", JOSA A, vol. 57, pp. 181-185.

47. **Andrews L. C., Al-Habash M. A., Yopen C. Y., Phili,ps R. L., (2001),** "*Theory of optical scintillation: Gaussian-beam wave model*", Waves Rand. Med., vol. 11, pp. 271-291.

48. **Eyyuboğlu H. T. and Bayraktar M.,(2015),** "*SNR bounds of FSO links and its evaluation for selected beams*", J. Modern Opt. vol. 62, no. 16, pp. 1316-1322.

49. **Yao M., (2009),** "*Scintillation index of astigmatic annular beams in a turbulent atmosphere*", I. J. Light and El. Opt., vol. 120, pp. 824-828.

50. **Eyyuboğlu H. T., (2013),** "*Scintillation behavior of Airy beam*", Opt. Laser Technol., vol. 47, 232-236.

51. **Eyyuboğlu H. T., (2015),** "*Per unit received power apertured averaged scintillation of partially coherent sinusoidal and hyperbolic Gaussian beams*", Opt. Laser Technol., vol. 71, 55-62.

52. **Eyyuboğlu H. T., (2013),** "*Scintillation analysis of hypergeometric Gaussian beam via phase screen method*",Opt. Commun., vol. 309, pp. 103-107.

53. **Eyyuboğlu H. T., (2013),** "*Estimation of aperture averaged scintillations in weak turbulence regime for annular, sinusoidal and hyperbolic Gaussian beams using random phase screen*", Opt. Laser Technol., vol. 52, 96-102.

54. **Eyyuboğlu H. T., (2013),** "*Apertured averaged scintillation of fully and partially coherent Gaussian, annular Gaussian, flat toped and dark hollow beams*",Opt. Commun., vol. 339, pp. 141-147.

55. **Öztan M. A., and Baykal Y. K., (2010),** "*Scintillation Index of Partially Coherent Asymmetrical Multi Gaussian Beams in Extremely Strong Turbulence*", Nat. Conf. on Elec. Electro. Comp. Eng., 11770183.

56. **Baykal Y. K., Eyyuboğlu H. T., Cai Y., (2008),** "*Incoherent sinusoidal-Gaussian and annular beam scintillations*", Proc. SPIE.

57. **Wang J., Yang J-Y., Fazal I. M., Ahmed N., Yan Y., Huang H., Ren Y., Yue Y., Dolinar S., Tur M., Willner A. E., (2012),** "*Terabit free-space data transmission employing orbital angular momentum multiplexing*", Nat. Phot, vol. 6, pp. 488-496.

58. **Fang Y., Yu J., Zhang J., Chi N., Xiao J., Chang G-K., (2014),** "*Ultrahigh-capacity access network architecture for mobile data backhaul using integrated W-band wireless and free-space optical links with OAM multiplexing*", Opt. Lett., vol. 39, pp. 4168-4171.

59. **Han J., Li L., Yi H., Shi Y., (2018),** "*1-bit digital orbital angular momentum vortex*
beam generator based on a coding reflective metasurface", Opt. Mat. Exp., vol. 8, pp. 3470-3478.

60. **Hsieh Y. H., Lai Y. H., Hsieh M. X., Huang K. F., Chen Y. F., (2018),** "*Generating high-power asymmetrical Laguerre-Gaussian modes and exploring topological charges distribution*", Opt. Exp., vol. 26, pp. 31738-31749.

61. **Zhang X., Tia T., Cheng S., Tao S., (2019),** "*Free-space information transfer using the elliptic vortex beam with fractional topological charge*", Opt. Commun., vol. 431, pp. 238-244.

62. **Shao W., Huang S., Liu X., Chen M., (2018),** "*Free-space optical communication with perfect optical vortex beams multiplexing*", Opt. Commun., vol. 427, pp. 545-550.

63. **Wang X., Yang Z., Zhao S., (2019),** "*Influence of oceanic turbulence on propagation of Airy vortex beam carrying orbital angular momentum*", I. J. Light and El. Opt., vol. 176, pp. 49-55.

64. **Cui X-Z., Yin X-L., Chang H., Guo Y-L., Zheng Z-J., Sun Z-W., Liu G-Y., Wang Y-J., (2018),** "*Analysis of an adaptive orbital angular momentum shift keying decoder based on machine learning under oceanic turbulence channels*", Opt. Commun., vol. 429, pp. 138-143.

65. **Guo Y., Cheng M., Dong K., (2018),** "*Characterizing turbulence-induced orbital angular momentum modes on Gaussian–Schell model beam in the atmosphere with wave-front correction*", I. J. Light and El. Opt., vol. 171, pp. 678-685.

66. **Cheng L., Hong W., Hao Z-C., (2014),** "*Generation of Electromagnetic Waves with Arbitrary Orbital Angular Momentum Modes*", Scie. Rep., vol. 4814, pp. 1-5.

67. **Li N., Chu X., Zhang P., Feng X., Fan C., Qiao C., (2018),** "*Compensation for the orbital angular momentum of a vortex beam in turbulent atmosphere by adaptive optics*", Opt. Laser Technol., vol. 98, pp. 7-11.

68. **Gou P., Kong M., Yang G-M., Guo Z-G., Zhang J., Han X., Xiao J., Yu J., (2018),** "*Integration of OAM and WDM in optical wireless system by radial uniform circular array*", Opt. Commun., vol. 424, pp. 159-162.

69. **Engay E., Banas A., Bunea A-I., Separa S. D., Glückstad J., (2019),** "Interferometric detection of OAM-carrying Helico-conical beams", Opt. Commun., vol. 433, pp. 247-251.

70. **Kai C., Feng Z., Dedo M. I., Huang P., Guo K., Shen F., Gao J., Guo Z., (2019**), "*The performances of different OAM encoding systems*", Opt. Commun., vol. 430, pp. 151-157.

71. **Li Y., Morgan K., Li W., Miller J. K., Watkins R., Johnson E. G., (2018),** "*Multi-dimensional QAM equivalent constellation using coherently coupled orbital angular momentum (OAM) modes in optical communication*", Opt. Exp., vol. 26, pp. 30969-30977.

72. **Mahdieh M. H. and Pournoury M., (2010),** "*Atmospheric turbulence and numerical evaluation of bit error rate (BER) in free-space communication*", Opt. Laser Technol., vol. 42, pp. 55-60.

73. **Cowan D. C. and Andrews L. C., (2008),** "*Effects of atmospheric turbulence on the scintillation and fade probability of flattened Gaussian beams*", Opt. Eng., vol. 47, pp.

74. **Toselli I., Andrews L. C., Philips R. L., Ferrero V., (2008),** "*Free-space optical system performance for laser beam propagation through non-Kolmogorov turbulence*", Opt. Eng. vol. 47, pp.

75. **Lyke S. D., Voelz D. G., Roggemann M. C., (2009),** "*Probability density of aperture-averaged irradiance fluctuations for long range free space optical communication links*", Appl. Opt. vol. 48, pp. 6511-6527.

76. **PoPoola W. O., (2009),** "*BPSK Subcarrier Intensity Modulated Free-Space Optical Communications in Atmospheric Turbulence*", J. Lightw. Technol., vol. 27, no.8, pp. 967-973.

77. **Anguita J. A., Djordjevic I. B., Neifeld M. A., Vasic B. V., (2005),** "*High-Rate Error-Correction Codes for the Optical Atmospheric Channel*" in Proceedings of SPIE, Free-Space Laser Communications V, Washington, USA, pp.

78. **Djordejevic I. B., Djordjevic G. T., (2009),** "*On the communication over strong atmospheric turbulence channels by adaptive modulation and coding*", Opt. Express, vol. 17, pp. 18250-18262.

79. **O'Brien D. C., (2005),** "Improving coverage and data rate in optical wireless systems", SPIE Proc. Free Space Laser Comm. V, vol. 5892.

80. **Luna R., Borah D.K., Jonnalagadda R., Voelz D. G., (2009),** "*Experimental Demonstration of a Hybrid Link for Mitigating Atmospheric Turbulence Effects in Free-Space Optical Communication*", IEEE Photon. Technol. Lett., vol 21, no. 17, pp. 1196-1198.

81. **Wang Z., Zhong W. –D., Fu S., Lin C., (2009),** "*Performance Comparison of Different Modulation Formats Over Free-Space Optical (FSO) Turbulence Links With Space Diversity Reception Technique*", IEEE Photon. J., vol. 1, no. 6, 276-285.

82. **Ren Y., Huang H., Xie G., Ahmed N., Yan Y., Erkmen B. I., Chandrasekaran N., Lavery M. P. J., Steinhoff N. K., Tur M., Dolinar S., Neifeld M., Padgett M. J., Boyd R. W., Shapiro J. H., Willner A. E., (2013),** "*Atmospheric turbulence effects on the performance of a free space optical link employing orbital angular momentum multiplexing*", Opr. Lett., vol. 38, no. 20, pp.4062-4065.

83. **Tyson R. K, Canning D. E., Tharp J. S., (2005),** "*Measurement of the bit-error rate of an adaptive optics, free-space laser communications system, part 1: tip-tilt configuration, diagnostics, and closed-loop results*", Opt. Eng., vol. 44, pp.

84. **Tyson R. K, Canning D. E., Tharp J. S., (2005),** "*Measurement of the bit-error rate of an adaptive optics, free-space laser communications system, part 2: multichannel configuration, aberration characterization, and closed-loop results*", Opt. Eng., vol. 44, pp.

85. **Ricklin J. C. and Davidson F. M., (2003),** "*Atmospheric optical communication with a Gaussian Schell beam*", J. Opt. Soc. Am. A, vol. 20, no. 5, 856-866.

86. **Chaman-Motlagh A., Ahmadi V., Ghassemlooy Z., (2009),** "A modified model of the atmospheric effects on the performance of FSO links employing single and multiple receivers", J. Mod. Opt., vol. 57, pp. 37-42.

87. **Andrews L. C. and Philips R. L.,(2004),** "*Free space optical communication link and atmospheric effects: single aperture and arrays*" in Proceedings of SPIE, Free-Space Laser Communication Technologies XVI, San Jose, Canada, vol. 5338.

88. **Bayraktar M., (2015),** "*Comparison of probability of error performance for truncated Bessel and Besssel Gaussian Beams*"*,* Grad. School of Nat. App. Sci.

89. **Kamacıoğlu C. and Baykal Y., (2012),** "*Generalized expression for optical source fields*", Opt. Las. Technol., vol. 44, pp. 1706-1712.

90. **Gradshteyn I. S. and Ryzhik I. M.,(2014),** "*Table of Integrals, Series and Products*", Academic Press, Massachusetts.

91. **Rao R., (2008),** "*Statistics of fractal structure and phase singularity of a plane light wave propagation in atmospheric turbulence*"*,* App. Opt., vol. 42, pp. 269-276.

92. **Bayraktar M. and Eyyuboğlu H. T., (2019),** "Propagation properties of optical bottle beam in turbulence", Opt. Eng., vol. 58, pp. 036104.

93. **Bayraktar M., (2019),** "Estimation of scintillation behavior and bit error rate analysis of sine hollow beam", OPTIK, vol. 188C, pp.147-154.

APPENDICES A

CURRICULUM VITAE

PERSONAL INFORMATION

Surname, Name: Bayraktar, Mert

Date and Place of Birth: 25 March 1990, Samsun

Marital Status: Single

Phone: +90 554 247 72 73

Email: mbayraktar@cankaya.edu.tr

EDUCATION

Degree	Institution	Year of Graduation
MSc	Çankaya Univ., Electronic and Communication Engineering	2015
B.Sc.	Çankaya Univ., Electronic and Communication Engineering	2013
B.Sc	Çankaya Univ., Computer Engineering (Double Major)	2013
High School	Tülay Başaran High School	2008

WORK EXPERIENCE

Year	Place	Enrollment
2014 - Present	Lazersan Haberleşme	Co-Founder
2013- Present	Çankaya Univ. Electronic and Communication Engineering	Research Assistant
2013 - Present	Lazersan Elektronik	Co-Founder
2012 July	Mikes	Intern
2012 June	Havelsan	Intern
2011 June	Türk Telecom.	Intern
2009 July	Walt Disney World	Life Guard

FOREIN LANGUAGES
Advanced English, Beginner Spanish, Beginner German

PUBLICATIONS

1. Bayraktar M., (2019), "Estimation of scintillation behavior and bit error rate analysis of sine hollow beam", OPTIK, vol. 188C, pp.147-154.
2. Bayraktar M. and Eyyuboğlu H. T., (2019), "Propagation properties of optical bottle beam in turbulence", Opt. Eng., vol. 58, pp. 036104.
3. Eyyuboğlu H. T. and Bayraktar M., (2016), "Propagation properties of cylindrical sinc Gaussian beam", J. Mod. Opt., vol. 63, pp. 1706-1712.
4. Eyyuboğlu H.T and Bayraktar M., "SNR bounds of FSO links and its evaluation for selected beams", J.Mod. Opt., vol 62. No 16, pp. 1316-1322, (2015).
5. Bayraktar, M., Başdemir, H. D., "*Cylindrical-Sinc Beam*", OPTIK, vol. 138, pp. 571-584, (2013).

PROJECTS

1. Visible Light Communication System, Project Number: 0082.TGSD.2014, Ministry of Science, Industry and Technology, 2014.

2. Free Space Optics Modem, Project Number: 0935.TGSD.2013, Ministry of Science, Industry and Technology, 2013.

HONOURS AND AWARDS

1. "Yeni Fikirler Yeni İşler 2014" compatition
   2st degree in category of Energy
2. "Yeni Fikirler Yeni İşler 2013" compatition
   1st degree in category of Defence Industry
3. "Yeni Fikirler Yeni İşler 2013 " compatition
   2st degree in category of Information Technology

4. Graduate High Honor Student 2013
   Çankaya University

HOBBIES
Travel, Books, Swimming, Fitness